Seasonal and tidal effects on water density gradients in the San Juan Channel

Katie Thomas[1]

Pelagic Ecosystem Function in the San Juan Archipelago Research Apprenticeship

Autumn 2011

[1]Friday Harbor Laboratories, University of Washington, Friday Harbor, WA 98250

Contact Information:
Katie Thomas
kthomas6@uoregon.edu

Keywords: San Juan Channel, physical oceanography, tidal mixing, pycnocline

Abstract

The San Juan Channel is one passageway linking the Strait of Georgia and the Strait of Juan de Fuca. Thus, the physical oceanography of this region is complex and has both estuarine and oceanic influences. We sampled a 5-station transect along the San Juan Channel during fall 2011 as part of a multi-annual study started in 2004 and a monthly study started in early 2011. We deployed a CTD to gather information on temperature, salinity, and density structure in the water column. Temperature followed an annual cycle with cooling in the winter and warming in the summer, while haloclines were more tidally modulated. Short-term along-channel density structure was controlled by both tides and wind. Density stratification increased at the south end increased during flood tides, and at the north end and mid-channel during ebb tides. The depth and width of the pycnocline at the southern end of the channel were correlated to tidal height. These findings enhance our understanding of both short-term and long-term patterns in density gradients of the San Juan Channel pelagic environment.

Introduction:

The San Juan Channel is one passageway that transports water between the Strait of Juan de Fuca and the Strait of Georgia (Figure 1). Along with the much larger Haro Strait to the west and Rosario Strait to the east, the San Juan Channel functions as a passageway in estuarine circulation (Foreman et al. 1995). While the Strait of Georgia connects to the ocean by the narrow Johnstone Strait in the north, virtually all circulation and oceanic input occurs via the Strait of Juan de Fuca and thus passes through the San Juan Channel and adjacent passageways (Masson 2002). Circulation follows a classic

estuarine model in which cool, saline oceanic water flows into the system at depth and warmer, fresher water flows out near the surface (Thomson 1994, Lie et al. 1998). This is driven by high freshwater input into the Strait of Georgia from the Fraser River (Thomson 1994, Masson 2002, Masson and Cummins 2004, Masson 2006). Overlaid on this consistent circulation pattern are strong transient currents driven by the mixed semidiurnal tides characteristic of the region (Thomson 1994, Lie et al. 1998, Masson 2006).

The bathymetry of the eastern Strait of Juan de Fuca and southern Strait of Georgia enhances tidal mixing in water passing from one basin to the other. A large sill extends southward into the Strait of Juan de Fuca from Victoria, B.C. (Herlinveaux and Tully 1961, Masson 2002), and another occurs northeast of the San Juan Channel and southwest of the Fraser River at Boundary Pass (Masson 2002). The sills physically obstruct tidal flows and lead to vigorous mixing downstream (Masson 2002). Thus, both the Strait of Georgia input into the north end of the San Juan Channel and the Strait of Juan de Fuca input into the south end are generally more mixed than their origin water masses (Herlinveaux and Tully 1961).

The degree of mixing at the sills is modulated by a biweekly spring to neap tidal cycle. During spring tides, flows are strong and water is pushed rapidly over the sill causing extensive turbulence. Deeper, denser water upstream of the sill becomes trapped and does not pass over, resulting in a warmer, fresher, highly mixed water column downstream of the sill (Davenne and Masson 2001). During neap tides, flows are weaker, and both shallow and deep water can ease over the sill without excessive mixing. The result is a more stratified water column with cool, salty water at depth downstream of the

sill (Davenne and Masson 2001). The tidal influence on deep-water renewal in both basins causes a spring-neap modulation of salinities that has been observed in the Haro Strait (Lie et al. 1998).

Mixing is also modulated by the shorter-term cycle of ebb and flood tides. During flood tides, water approaching the Strait of Georgia becomes highly mixed and virtually homogenous, while during ebb tides stratification emerges and fresh Fraser River surface water can flow out of the system (Tully and Dodimead 1957). This trend has been observed at the north end of San Juan Channel (Bernard 2010). Flood tide may increase mixing near the bottom because the denser oceanic water moving landward interacts with bottom roughness and causes turbulence (Waldichuk 1957). However, Cudaback and Jay (2000) developed a mathematical estuarine model in which bottom friction reduced vertical shear in the water column and decreased the width of the pycnocline, while the lack of friction during ebbing tides increased vertical shear and caused mixing in the water column, increasing the width of the pycnocline. Data from the Columbia River estuary closely matched model predications (Cudaback and Jay 2000). Pycnocline depth moved up and down with tidal height, which has also been observed at the south end of San Juan Channel where waters are consistently stratified (Cudaback and Jay 2000, Bernard 2010). Thus, ebb and flood tides may affect mixing differently depending on initial stratification, bottom roughness, and vertical shear.

In addition to short-scale tidal changes, the San Juan Channel is subject to seasonal changes in physical oceanography that result from processes such as variations in freshwater input and shifts in coastal wind regimes (Thomson 1994). Freshwater runoff from the Fraser River peaks in early summer, causing high stratification in the

Strait of Georgia, while during the winter water is more homogenous (Waldichuk 1957, Masson 2002). Winter brings strong southeasterly winds that cause coastal downwelling, which brings less dense oceanic water into the system through the Strait of Juan de Fuca. Summer brings strong northwesterly winds that cause coastal upwelling, which brings colder, saltier oceanic water into the system (Masson 2006). The shift from summer upwelling to winter downwelling is known as the fall transition and leaves a noticeable signature on deep water in the south end of the San Juan Channel (Bernard 2010).

The purpose of this study was to understand long-term seasonal trends in temperature and salinity and short-term tidal impacts on mixing in the San Juan Channel by addressing the following questions: (1) How do vertical profiles of salinity and temperature at North and South Stations change in an annual cycle, (2) how does tidal phase affect mixing along the length of the Channel, and (3) what are tidal impacts on the width and depth of the pycnocline at the South Station?

Methods:

Data collection:

Oceanographic data were collected in autumn 2011 by the Pelagic Ecosystems Function Research Apprenticeship program (PEF) at Friday Harbor Laboratories during approximately weekly cruises throughout October and November. This added to a full-year dataset for 2011 sampled almost monthly in collaboration with the Northwest Indian College and Western Washington University.

A 5-station transect was sampled aboard the University of Washington's R/V Centennial, starting at the south end of the San Juan Channel and ending at the north

(Figure 1). Occasionally, select stations were not sampled due to weather conditions or time constraints. Sample dates and stations are summarized in Table 1. At each station, a Seacat Model SBE-19 CTD mounted on a rosette was deployed using standard operating procedures from the surface to approximately 10m above the bottom to collect data on conductivity, temperature, and depth through the water column. Raw CTD data were processed using SBEDataProcessing software according to standard operating procedures developed by Jan Newton for the Joint Effort to Monitor the Strait in accordance with the University of Washington and Washington Department of Ecology procedures.

Data analysis:

Seasonal characterization of physical oceanography:

All data from 2011 (February-November) were used to assess seasonal changes in salinity and temperature in the channel. Haloclines, thermoclines, and pycnoclines at South and North stations were plotted in Excel. Upwelling indices from La Push, WA (125W, 48N) were obtained from the NOAA Pacific Fisheries Environmental Laboratory (http://www.pfeg.noaa.gov/products/current_products.html) and graphic representations of data were provided by the Columbia River DART website from the University of Washington (http://www.cbr.washington.edu/dart/upwell.html).

Along-channel mixing:

Contour plots were made in SigmaPlot (Version 11.0) to examine density variation along the full transect for each cruise date during fall 2011. Tidal and meteorological data were accessed from NOAA online (http://tidesandcurrents.noaa.gov/)

for the Friday Harbor, WA station (9449880) and compared to contour plots. Temperature-salinity (T-S) profiles were constructed in Excel for each station during fall 2011. Redfield's (1950) characteristic water mass temperatures and salinities were superimposed onto T-S plots to determine water origins. Standard deviation of density was used as a proxy for level of stratification and was calculated at each station for each cruise in fall 2011.

Tidal effects on the pycnocline:

Pycnocline depth and width analysis was performed only on the South station, as this station maintained a consistent pycnocline throughout fall 2011. Standard equations for measuring oceanic pycnoclines could not be used in this study because of high variability in pycnocline characteristics and the frequent presence of discrete layered pycnoclines. To account for this, the pycnocline was considered to span the entire region from the shallowest point of rapidly changing density to the deepest, including any mixed regions between. The upper and lower limits were defined by a change in density $\geq$ 0.02Kg/m^3 for $\geq$ 3 consecutive 0.5m depth bins. This method produced upper and lower limits that closely matched limits estimated from visual examination of vertical profiles (Figure 2). The width of the pycnocline was defined as the distance between the upper and lower pycnocline limits, and the depth defined as the midpoint between the upper and lower limits (Figure 3). Pycnocline depth and width were plotted against tidal height in Excel, and linear regressions were run to determine correlation coefficients.

Results:

Upwelling and downwelling regimes, 2011:

During fall 2011 sampling (4 October to 19 November), coastal wind regimes were indicative of coastal downwelling, with a brief upwelling episode in mid-November (Figure 4). Coastal upwelling indices from January to November 2011 showed a winter downwelling regime from January through early April, a summer upwelling regime from early April through mid-September, and a downwelling regime mid-September through November (Figure 5).

Temperature and salinity cycles, 2011:

Plots of thermoclines at South Station throughout 2011 showed a cycle of cooling in the winter and warming in the spring and summer (Figure 6). Surface waters were coolest in March and February, and progressively warmed until maximum surface temperatures were observed in August. Eight cruises from early October to late November showed progressively cooler surface waters. High stratification was observed in July and August, while February and April showed a more well-mixed temperature structure. Deep water at South station was coolest in February and April, and warmest in October. Plots of haloclines at South Station did not show a clear seasonal cycle in salinity structure; however, the lowest salinities in the upper 50m of the water column were observed in August, April, and February (Figure 7).

Plots of thermoclines at North Station for throughout 2011 (Figure 8) showed the same annual temperature cycle observed at South Station, with cooler temperatures early in February and March, peak surface temperatures in July and August, and a transition back into cooling through October and November. North Station temperatures were

mostly isothermal, with the exception of July and August, which had relatively warm surface water and cold deep water. Haloclines at North Station (Figure 9) were highly variable and did not display a clear progression over time. However, during the summer months sampled (July and August) there were strong freshwater signals in the upper 20m of the water column while there was relatively high salinity water at depth (Figure 10). North Station exhibited stronger stratification in salinity than in temperature.

Tidal effects on vertical profiles, Fall 2011:

South Station haloclines (color-coded by tidal phase) showed higher salinities in the upper 30m of the water column during ebb tides, and lower salinities during flood and slack high tides (Figure 11). The opposite trend was observed in deep water. The most saline deep water (below 70m) was observed during the two flood tides sampled during neap cycles in November. The two flood tides sampled in October were also during neap cycles, but had less saline deep water. Thermoclines at South Station did not display a clear trend with regard to flood and ebb tidal phase (Figure 12).

North Station haloclines showed higher salinity deep water during flood tides than during ebb tides, although a halocline from slack high had the second lowest salinity deep water (Figure 13). Lowest salinities were observed during an ebb tide, but a fresh surface signal was also observed during a slack high.

Temperature-salinity profiles Fall 2011:

Temperature vs. salinity (T-S) plots for South Station showed a seasonal fall trend from warmer, less saline water to cooler, more saline, and more mixed water (Figure 14).

T-S ranges were characteristic primarily of a mixture of water originating from the Strait of Juan de Fuca (JdF), Strait of Georgia (SG), and surface Pacific Ocean (PO) according to Redfield's (1950) water mass origins. South Station deep water also showed T-S relationships characteristic purely of surface PO water early in the season, and mid-depth PO water later in the season. T-S plots for station C showed the same temperature progression from warmer to cooler water throughout the fall season (Figure 15). Water was more mixed at Station C than at South Station, and all T-S lines fell within a mixture of JdF, GS, and surface PO water. At Station B, water was more well-mixed than Station C, and the majority of T-S relationships were characteristic of a mixture of JdF, GS, and surface PO origins (Figure 16). On 18 October Station C had primarily JdF and SG origins and was less mixed. Station A T-S plots showed high mixing and similar water origins to Station B, and on 18 October water characteristic of surface GS origins was observed (Figure 17). North Station T-S plots, similar to South Station, showed decreasing temperature and increasing mixing throughout the season (Figure 18). North Station showed the most surface GS and mixed JdF and GS water origins of any station, and had the highest temperatures and lowest salinities of the transect.

Along-channel density structure, Fall 2011:

The transect was completed during flooding tides on 7 October, 24 October, and 7 November (Figure 19). Contour plots of along-channel density showed a high-density concentration at the depths of South Station and Station C and a low-density concentration in North Station surface water on all three dates. A low-density concentration was also evident in South Station surface water, and had a stronger signal

during the higher-exchange flood tides on 7 and 24 October than on the lower-exchange flood tide on 7 November.

The transect was completed during ebbing tides on 18 October, 1 November, and 15 November (Figure 20). The penetration of the North Station low-density surface concentration into the mid-channel was highly variable, and higher exchange ebb tides did not result in a stronger mid-channel, low-density signal. On 18 October, the low-density surface signal in mid-channel was strongest, after the region experienced persistent northerly winds for 24 hours prior to sampling (Figure 21). On 15 November, low-density surface water was less extreme, but still extended across the channel to Station C, after the region experienced primarily east winds but also some intermittent northerly winds and almost no southerly winds in the 48 hours prior to sampling. On 1 November, when little low-density signal was observed, winds were primarily southeast with few north winds in the 24 hours prior to sampling, and 60 hours before sampling south winds were predominant.

Tidal effects on along-channel density stratification, Fall 2011:

Standard deviation of density plotted against cruise number for fall 2011 showed that South Station consistently has the most stratified water column (Figure 22). North Station was the next most stratified station. Mid-channel stations were all highly mixed, but Station C was generally more stratified than Stations A and B.

At South Station, more stratification was observed during flood tides than during ebb tides (Figure 23). At Station C, flood tides and ebb tides showed similar standard deviations of density, except for during an ebb tide during the third cruise (18 October),

when density stratification was over three times as strong as all other cruise dates (Figure 24). Station B low standard deviations of density, but showed increased stratification during ebb tides (Figure 25). Station A was also well-mixed but had the most stratification during ebb tides (Figure 26). North Station had highest stratification during the ebb tide on cruise 3 (18 October), but on other cruise dates did not show a clear tidal pattern in standard deviation of density (Figure 27).

Tidal variation and the South Station pycnocline, 2011

Pycnocline structure at South Station was highly variable during all months in 2011, and often two or more discrete pycnoclines occurred with a mixed layer in between (Figure 28). During fall 2011, pycnocline depth and width changed substantially between cruise dates (Figure 29). Tidal phase did not have a clear relationship with pycnocline depth throughout 2011 (Figure 30). However, in the fall season (October and November), the pycnocline was deepest during flood tides. Pycnocline width was greatest during flood or slack high tides throughout 2011 (Figure 31). However, the thinnest pycnocline observed was also during a flood tide, and was very similar to the width of an ebb tide pycnocline in the same month (November).

For fall 2011 sample dates, depth of the pycnocline at South Station correlated to tidal height (R^2=0.3294) (Figure 32). However, when data from earlier months in 2011 were included no correlation between tidal height and depth of the pycnocline was found (R^2=0.0678) (Figure 33). The most extreme outliers on the linear regression of full-year data were August and February cruise dates (Figure 34). For fall 2011 sample dates, width of the pycnocline at South Station correlated strongly to tidal height (R^2=0.7819)

(Figure 35). When data from earlier in the year were included, the correlation remained strong (R^2=0.7278) (Figure 36). Data from all months fit the linear regression well, but minor outliers occurred in February and November (Figure 37).

Discussion:

Seasonal trends and annual cycles in physical oceanography

Spring and fall transitions in coastal wind regimes affect the water that is delivered to the San Juan Channel via the Strait of Juan de Fuca and have important ecological effects. Coastal upwelling indices at the oceanic entrance to the Strait of Juan de Fuca were indicative of a downwelling regime during our cruises in fall 2011 (Figure 4). Consistent with this data, we did not observe a distinct shift in South Station salinities at depth during the fall as past PEF apprentices have found before and after the fall transition (Bernard 2010). Further analysis of coastal upwelling indices from all of 2011 show that winter downwelling continued through early April, when the spring transition to an upwelling regime occurred (Figure 5). The fall transition back into a downwelling regime occurred in mid-September. Bernard (2010) found that physical effects of the fall transition were observed in San Juan Channel about a week after observed changes in coastal wind regime. Thus, even with the lag time between coastal processes and the delivery of oceanic water to the San Juan Channel through the Strait of Juan de Fuca, the fall transition likely occurred in our study region during mid to late September, well before our first fall cruise on 4 October.

The timing of the fall transition in 2011 was very early compared to cumulative 2005 to 2010 observations (see Bernard 2010, Table 3). The average day of the fall

transition from 2005-2010 was 17 October, and in 2006-2010 the fall transition ranged from mid-October to early November. The early transition in 2011 is not unprecedented; in 2005 the fall transition occurred around 27 September (Bernard 2010).

Thermoclines at both South (Figure 6) and North (Figure 8) Stations exhibited an annual cycle in the upper water column of cooling through March, warming through August, and then cooling again through November. Past work in the Strait of Juan de Fuca found an annual cycle in surface waters with coolest temperatures around February and highest temperatures ranging from June to August (Herlinveaux and Tully 1961), which is consistent with our observations in 2011. At both stations, temperatures were most isothermal in February and March and most stratified in July and August. Waldichuk (1957) found that the Strait of Georgia tends to become homogenous in the winter due to tidal mixing and reduced freshwater input, whereas it becomes more stratified in the summer during freshwater intrusions and becomes stable enough to remain stratified during tidal mixing. This pattern is consistent with our 2011 observations.

Haloclines at South (Figure 7) and North (Figure 9) Stations did not exhibit a distinct annual cycle of salinities, except for a strong freshwater signal at North Station in July and August (Figure 10). This was likely due to Fraser River discharge. Since salinity structure at both stations did not show clear trends at a monthly resolution, salinity structure may be mediated more by shorter-scale drivers, such as tides and wind.

During fall 2011 cruises, South Station thermoclines did not exhibit a pattern with tidal phase (Figure 12); thermoclines got progressively cooler throughout the fall regardless of tide (Figure 6). However, South Station surface salinity was higher during

ebbing tides than during flooding tides (Figure 11). Only two ebbing tides were sampled, which limits broad assumptions, but this pattern may result from the advection of low-salinity Puget Sound water to South Station during flooding tides.

In deeper South Station water, the most saline deep water occurred during flood tides. This is consistent with known estuarine circulation in the region, in which dense, high saline oceanic water flows in near the bottom during flood tides (Thompson 1994). However, two flood tides sampled had lower salinity deep water, which complicates this explanation. This difference could be a seasonal trend, as the lower salinity observations were both during October, and the higher salinity observations both in November. Streitenberger (2009) found that from 2004 to 2009, South Station salinity at depth was variable over the fall season and did not show a consistent seasonal trend, although Bernard (2010) found that after the fall transition, deep water showed a distinct decrease in salinity in 2010.

After the fall transition in September of 2011, we would expect to see lower-salinity deep water from coastal downwelling coming through the Strait of Juan de Fuca to South Station, but we observed an opposite temporal trend. A brief upwelling event occurred in mid-November (Figure 4), but one of the high-salinity observations occurred before it on 7 November and one shortly after on 19 November, so it is unlikely that upwelled waters had time to travel to South Station from the coast (Figure 11). These observations could also be attributed to deep-water intrusion over the Victoria Sill and into the inner portion of the Strait of Juan de Fuca, which delivers deep water to the South Station. Deep, and thus coldest and most saline, water from the Strait of Juan de Fuca gets trapped on the east side of the Victoria sill during spring tides due to high-

speed currents, but during especially slow neap tides can ease over the sill and enter the inner Juan de Fuca basin (Masson 2002). Temperature-salinity plots for South Station (Figure 14) show that November sample dates have more deep water of oceanic origin than October sample dates, which supports the hypothesis of a deep-water intrusion. Future work with the PEF dataset could further analyze fall seasonal trends in deep water salinity at South Station to address the relative importance of the fall transition and deep water intrusions over the Victoria sill.

During fall 2011, North Station deep water was more saline during flood tides than during ebb (Figure 13). This is likely because flood tides carry deep, high salinity water from the Strait of Juan de Fuca through the San Juan Channel. During one fall cruise, North Station was sampled just at slack high. We would expect slack high to resemble flooding tides, because it results from a flood tide, yet bottom water at North Station was low-salinity. This could be due to low stratification during the sample-time; the water column was nearly isohaline from 40 m to the bottom, so high salinity bottom water may have been mixed into the water column and lost its signature.

Water masses have characteristic temperature-salinity properties, and plotting temperature vs. salinity in an area with high levels of mixing, like the San Juan Channel, can help reveal likely water origins (Redfield 1950). Temperature-salinity plots for each station along the channel in fall 2011 (Figures 14-18) showed a gradual transition from the south end, where more oceanic origin water was observed, to the north end, where Strait of Georgia surface origin water was observed. In between was a mixture of oceanic surface, Strait of Juan de Fuca, and Strait of Georgia origin water. This observation is what we would expect, given that the south end of San Juan Channel opens toward the

Strait of Juan de Fuca, while the North end opens toward the Strait of Georgia (Figure 1). Mid-channel stations had smaller ranges of temperatures and salinities due to high levels of mixing. Bathymetric shoaling in the mid-channel, such as Reid Rock near Station A, shoaling between stations A and B, and a sill at Cattle Pass between South Station and Station C, increases turbulence during tidal exchange and causes the high levels of mixing observed in the mid-channel region.

Tidal effects on along-channel mixing

Along-channel contour plots of density revealed that density structure is mediated by both tides and wind (Figures 19-21). During flooding tides, the south end of the channel has a low-density concentration at the surface, and this pattern is stronger during higher-exchange tides (Figure 19). This is likely due to the advection of surface water from the Puget Sound during flood tides. During ebbing tides, there is no low-density surface water signature at the south end of the channel, and the low-density surface waters at the north end penetrate the mid-stations to highly variable degrees (Figure 20). This variability is consistent with forcing by wind patterns (Figure 21). During persistent north winds, low density water at the north end of the channel, likely from the Fraser River plume, was advected southward and aided by ebbing tidal currents. When winds were not as persistent from the north, low-density water had a diminished presence in the channel. When winds were not northerly, the mid-channel had no low-density signal from the north. Fraser River freshwater input has a substantial effect on salinity structure at the north end of the channel (Kull 2008). Because of the Fraser River plume, the north end of the channel may be more influenced by local wind patterns than the south end. The

observation that both wind and tides affect density structure in the Georgia-Fuca system is consistent with mathematical model predictions for the area (Masson and Cummins 2000).

Standard deviation of density was used as a proxy for mixing at all stations during fall 2011, with higher standard deviations indicating a more stratified water column. South Station consistently had the most stratification and North Station the second most (Figure 22). Station C was the most stratified of the mid-channel stations, and Stations B and A were highly mixed and had similar standard deviations of density across cruises. High mixing within the channel can be attributed to highly variable bathymetry and high speeds of water jetting through the channel and causing extensive turbulence.

South Station was more stratified during flood tides than ebb tides (Figure 23) because stratification at the south of the channel results mostly from high density deep water that is replenished during flood tides. Stations C, B, A, and North Station were most stratified during ebb tides (Figures 24-27). Stratification at North Station is driven by low-density Strait of Georgia surface water, which is pushed into the channel during ebb tides and increases stratification across the mid-stations. Thus, while different tidal current directions stratify different stations, density structure is tidally modulated across the San Juan Channel.

Tidal effects on density structure

South Station is the only station that remained consistently stratified, so an analysis of tidal effects on the pycnocline was not useful at other stations. At South Station, a stratified pycnocline was observed during all cruises in 2011 (Figure 28).

Pycnocline depth and width was highly variable during weekly cruises in fall 2011, indicating that a short-scale driver, such as tides, influences pycnocline structure (Figure 29). Throughout 2011, no strong patterns between flood or ebb tides and pycnocline depth (Figure 30) or width (Figure 31) were found. Using tidal height rather than ebb and flood categories better explained the depth and width of the pycnocline.

During fall 2011, the depth of the pycnocline at South Station was fairly well-correlated to tidal height (R^2=0.3294) (Figure 32). Bernard (2010) found a slightly stronger correlation (R^2=0.5595) for fall 2008-2010. These values are not directly comparable because a different method of determining the depth of the pycnocline was used in each analysis, but they are relatively consistent and together strongly support that the pycnocline moves up and down in the water column with tidal height to some degree during the fall season.

When data from all months sampled in 2011 were included, the depth of the pycnocline was no longer correlated to tidal height (R^2=0.0678, Figure 33). Strong outliers were observed in February and August (Figure 34). In February this was likely due to high levels of mixing that pushed the thermocline deeper than any other date observed and may not have been tidally modulated (Figure 28). For example, winter storms can extensively mix the upper water column. The August outlier was likely due to the fact that nearly the entire water column was a gradual pycnocline, making a measure of pycnocline depth meaningless and potentially unchanged with tidal height (Figure 28). While tidal height may have an impact on pycnocline depth year-round, confounding factors such as non-tidal mixing and extreme summer stratification may obscure the relationship in earlier months.

During fall 2011, the width of the pycnocline was strongly correlated to tidal height at South station (R^2=0.7819) (Figure 35). This relationship held when data from earlier in 2011 was considered (R^2=0.7278) (Figure 37). The relationship between pycnocline width and tidal phase has been documented in the Columbia River estuary and accurately predicted by a mathematical model (Cudaback and Jay 2000). During flooding tides in an estuary, water rushes in along the bottom, and bottom friction causes turbulence that slows incoming water. This reduces the vertical shear of the water column, which allows the pycnocline to thin. Since flooding leads to high tide, the pycnocline is thinnest at high tide. During ebbing tides, water exits the system near the surface and encounters relatively less friction, so vertical shear is increased. This leads to mixing within the water column, which thickens the pycnocline. Since low tide follows ebbing, the pycnocline is thickest at low tide (Cudaback and Jay 2000). The observed correlation between pycnocline width and tidal height in the San Juan Channel is consistent with Columbia River observations, which suggests that this relationship may be widespread and support the Cudaback and Jay (2000) model of estuarine tidal mixing.

Conclusions

This research provided new insights into annual oceanographic cycles and short-term drivers of density gradients in the San Juan Channel. Key observations were as follows: (1) Both ends of the channel exhibited a distinct annual cycle in temperature and displayed persistent cooling through the fall, while salinity did not and may be tidally modulated at both ends of the channel. (2) Compared to previous years, 2011 had a very early fall transition. (3) Consistent with prior years, water at South Station had more

oceanic origins, while North Station had more Strait of Georgia influence. (4) Along-channel stratification is modulated by tides and wind, and stratification increases during flood tides at South Station and during ebb tides at North Station and mid-channel. Finally, (5) tidal height influences the depth and width of the pycnocline at South Station. Further research incorporating Pelagic Ecosystem Function data from 2004-2010 into these analyses would strengthen these conclusions and provide a better understanding of density gradients in the San Juan Channel.

Acknowledgements:

This work could not have been completed without the ample help of my fellow apprentices, and particularly my fellow oceanographic researchers Brigitte Meyer, Derek Blackstone, and Bridget Bradshaw. Jan Newton, Breck Tyler, and Connie Sullivan taught data collection methods and gave invaluable feedback on analysis and early drafts of this paper. Our cruise captains Wolf, Dennis, and Mark facilitated successful and entertaining cruises. Ryan McLoughlin created the PEF database and provided support in data analysis. Finally, our partnership with the Northwest Indian College and Western Washington University provided us with winter, spring, and summer data that were essential for this analysis.

References:

Bernard GA. 2010. Effects of tides and remote forcing on oceanographic properties within the San Juan Channel during early fall. University of Washington, Friday Harbor Labs: 1-22.

Davenne E, Masson D. 2001. Water properties in the Straits of Georgia and Juan de Fuca. Institute of Ocean Sciences, Sidney, BC:1-41.

Foreman MGG, Walters RA, Henry RF, Keller CP, Dolling AG. 1995. A tidal model for eastern Juan de Fuca Strait and the southern Strait of Georgia. Journal of Geophysical Research 100:721-740.

Herlinveaux RH, Tully JP. 1961. Some oceanographic features of Juan de Fuca Strait. Journal of the Fisheries Research Board of Canada 18(6):1027-1071.

LeBlond PH, Ma H, Doherty F, Pond S. 1991. Deep and intermediate water replacement in the Strait of Georgia. Atmosphere-Ocean 29(2):288-312.

Li M, Garget A, Denman K. 1998. Seasonal and interannual variability of estuarine circulation in a box model of the Strait of Georgia and Juan de Fuca Strait. Atmosphere-Ocean 37(1):1-19.

Masson D. 2002. Deep water renewal in the Strait of Georgia. Estuarine, Coastal, and Shelf Science 54:115-126.

Masson D. 2006. Seasonal water mass analysis for the straits of Juan de Fuca and Georgia. Atmosphere-Ocean 44(1):1-15.

Masson D, Cummins P. 2004. Observations and modeling of seasonal variability in the Straits of Georgia and Juan de Fuca. Journal of Marine Research 62:491-516.

McLaughlin R. 2009. Inter-annual variation in temperature, salinity, and dissolved oxygen in San Juan Channel: patterns and external driving forces. University of Washington, Friday Harbor Labs: 1-28.

Redfield AC. 1950. Notes on the circulation of a deep estuary. Proceedings of the Colloquium on the Flushing of Estuaries. Woods Hole Oceanographic Institution.

Streitenberger C. 2009. Influence of external factors on interannual variability of physical oceanographic properties within the San Juan Archipelago. University of Washington, Friday Harbor Labs: 1-29.

Thomson RE. 1994. Physical oceanography of the Strait of Georgia-Puget Sound-Juan de Fuca Strait System. Canadian Technical Report of Fisheries and Aquatic Sciences No. 1948.

Tully JP, Dodimead AJ. 1957. Properties of the water in the Strait of Georgia, British Columbia, and influencing factors. Journal of the Fisheries Research Board of Canada 14(3):241-319.

Waldichuk M. 1957. Physical oceanography of the Strait of Georgia, British Columbia. Journal of the Fisheries Research Board of Canada 14(3):321-486.

Table 1: Cruise dates and stations sampled by PEF and partners 2004-2011

Year	Sample date	Stations sampled				
		S	**C**	**B**	**A**	**N**
2011	10-Feb	x				x
	08-Mar	x	x	x	x	x
	26-Apr	x	x	x	x	x
	08-July	x	x	x		x
	19-July		x	x	x	x
	21-July					x
	09-Aug	x				x
	04-Oct		x	x	x	x
	07-Oct	x	x	x	x	x
	18-Oct	x	x	x	x	x
	24-Oct	x	x	x	x	x
	01-Nov	x	x	x	x	x
	07-Nov	x	x	x	x	x
	15-Nov	x	x	x	x	x
	19-Nov	x				x

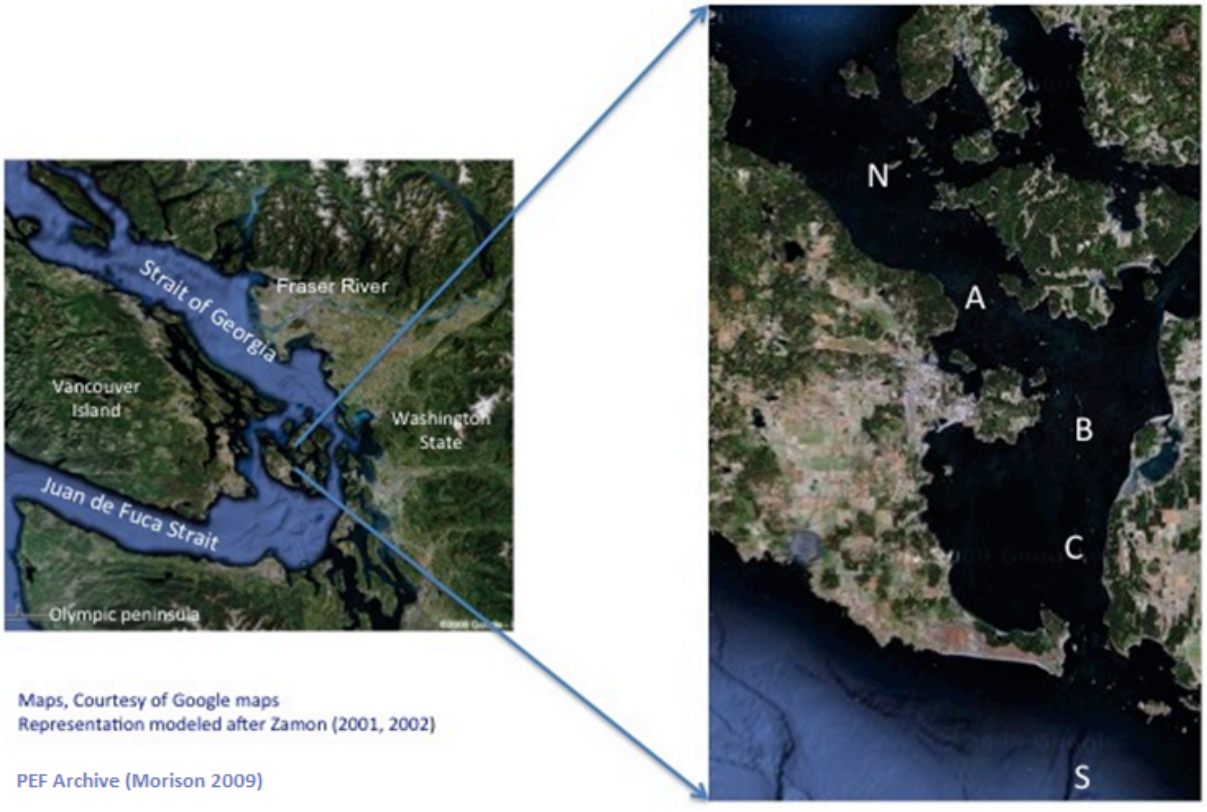

Figure 1: Station locations and names, from Bernard (2010). Precise station locations are as follows: S (48 25.200 N, 122 56.600 W), C (48 28.991 N, 122 57.470 W), B (48 31.398 N, 122 56.704 W), A (48 32.709 N, 122 58.746 W), N (48 35.000 N, 123 02.500 W).

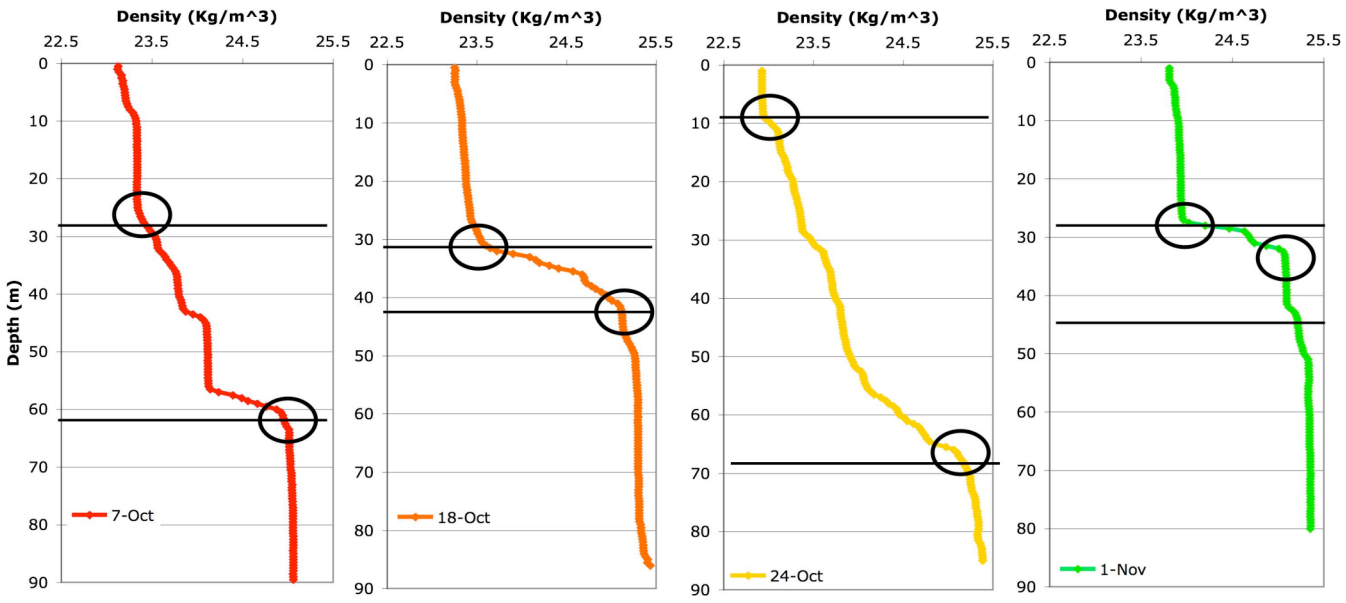

Figure 2: Example of pycnocline upper and lower limits determined by visual estimation (circles) and formula (lines).

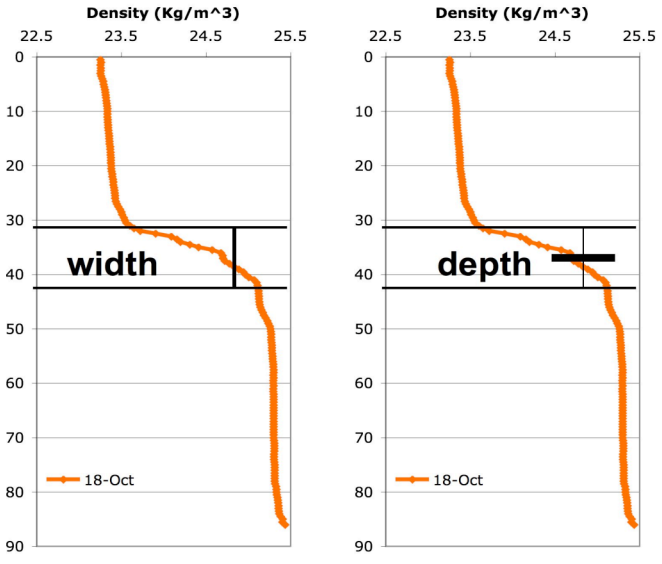

Figure 3: Example of the width and depth of the pycnocline at South Station.

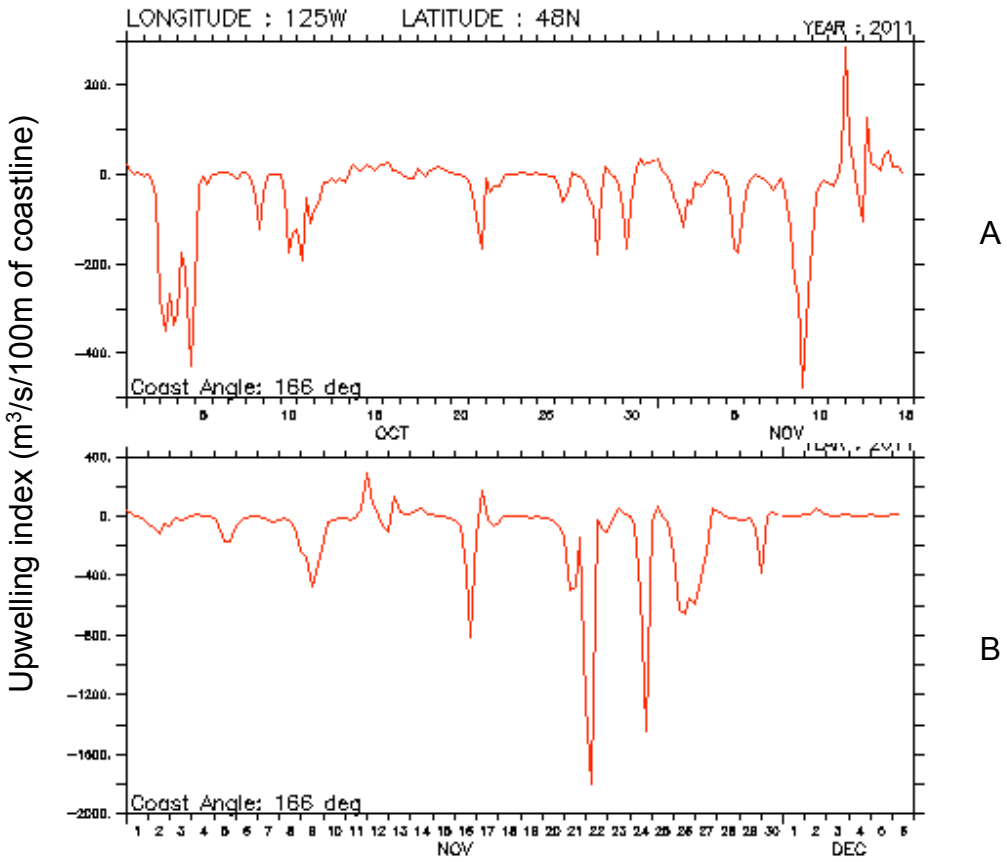

Figure 4: Upwelling index vs. date for (A) October and (B) November 2011 at 125W, 48N. Note that the x-axis scale changes between figures A and B. Positive indices indicate upwelling and negative indices downwelling. Graphs courtesy of NOAA.

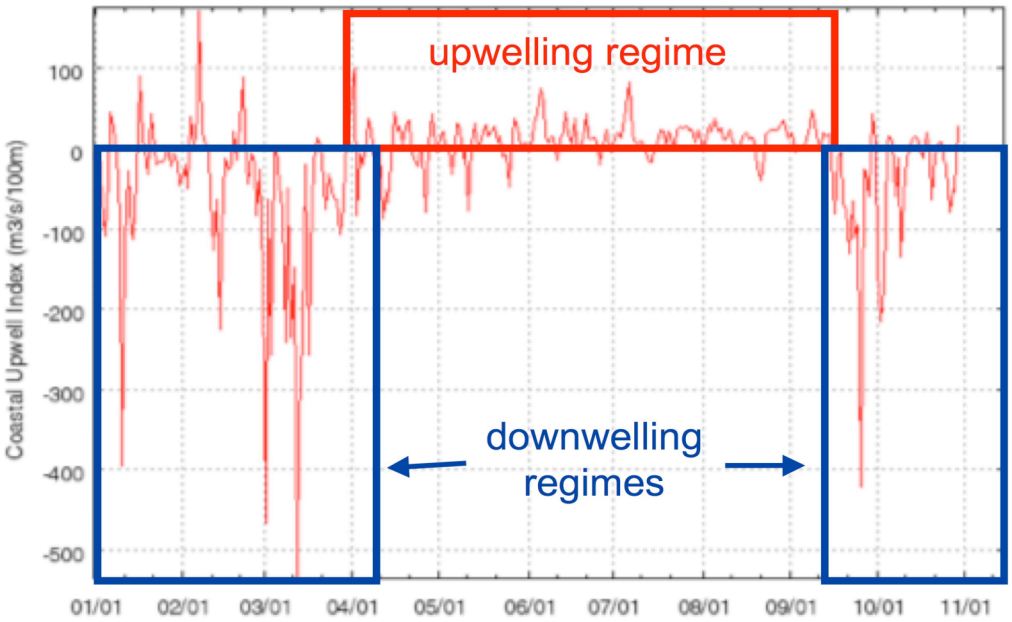

Figure 5: Upwelling index vs. date for 2011 at 125W, 48N. Positive indices indicate upwelling and negative indices downwelling. Winter downwelling continued through early April, when the spring transition to an upwelling regime occurred. The fall transition back into a downwelling regime occurred in mid-September.

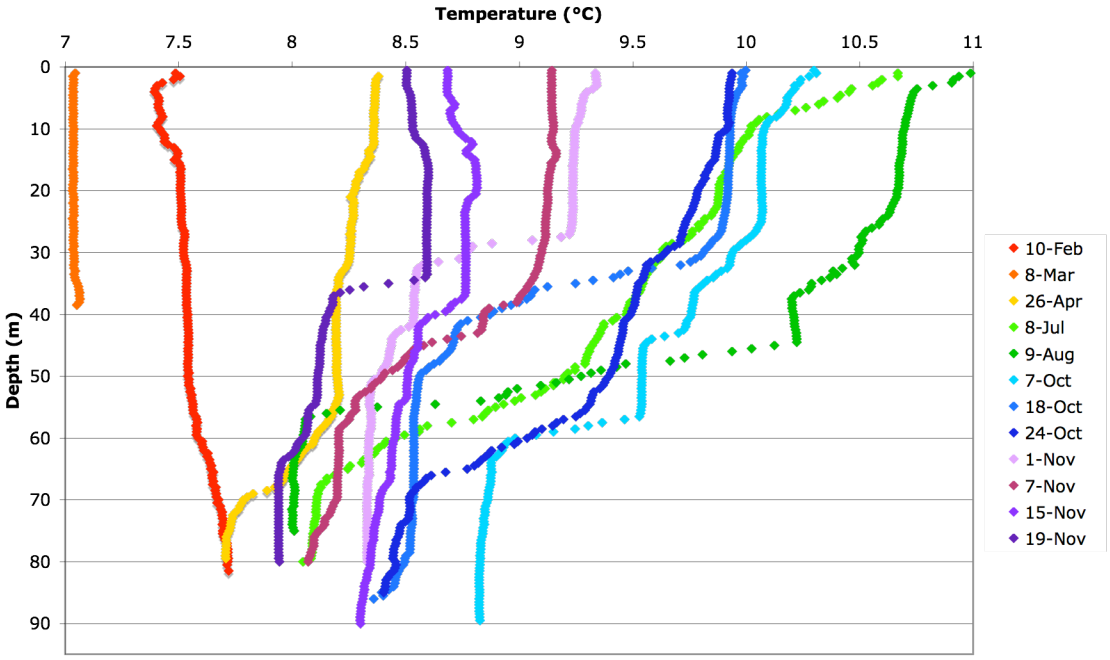

Figure 6: Thermoclines at South Station for all of 2011

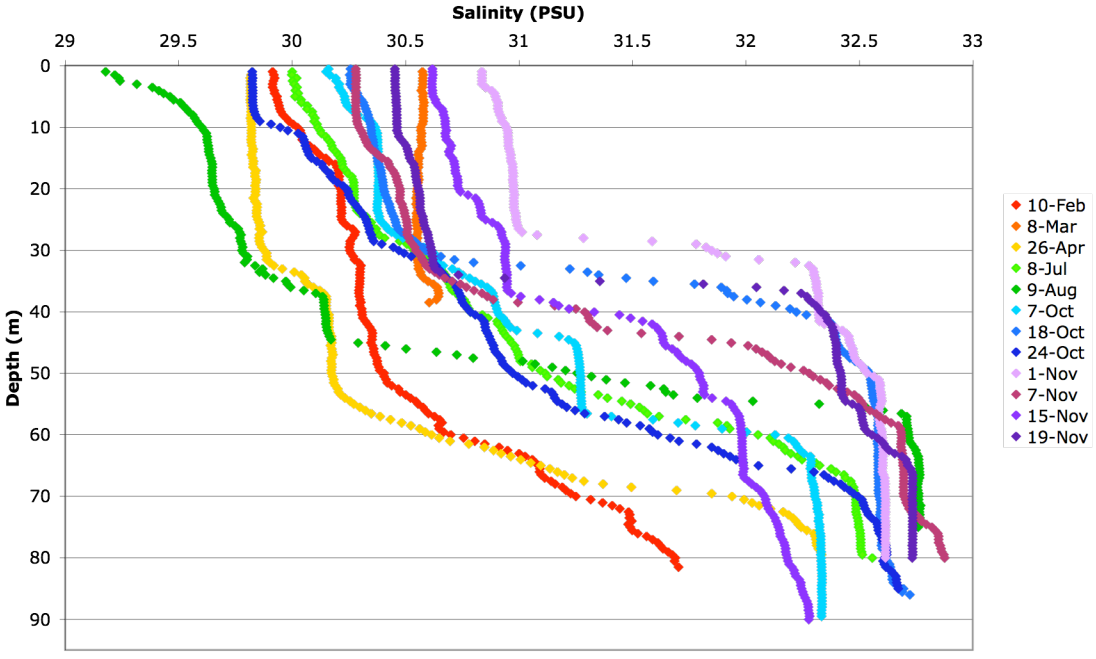

Figure 7: Haloclines at South Station for all of 2011

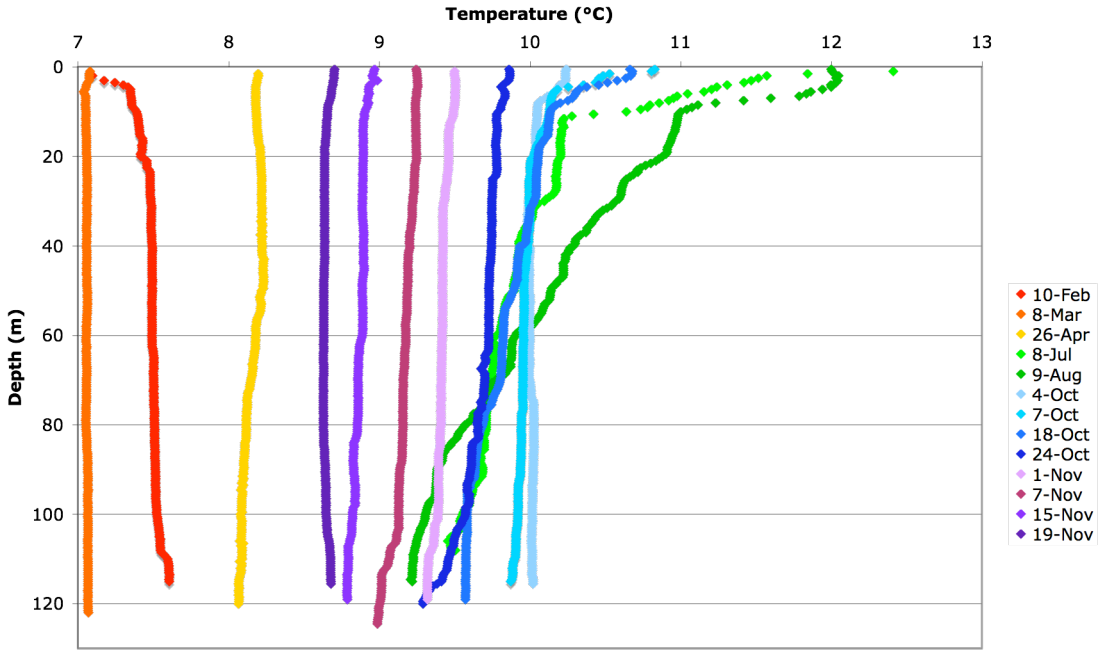

Figure 8: Thermoclines at North Station for all of 2011

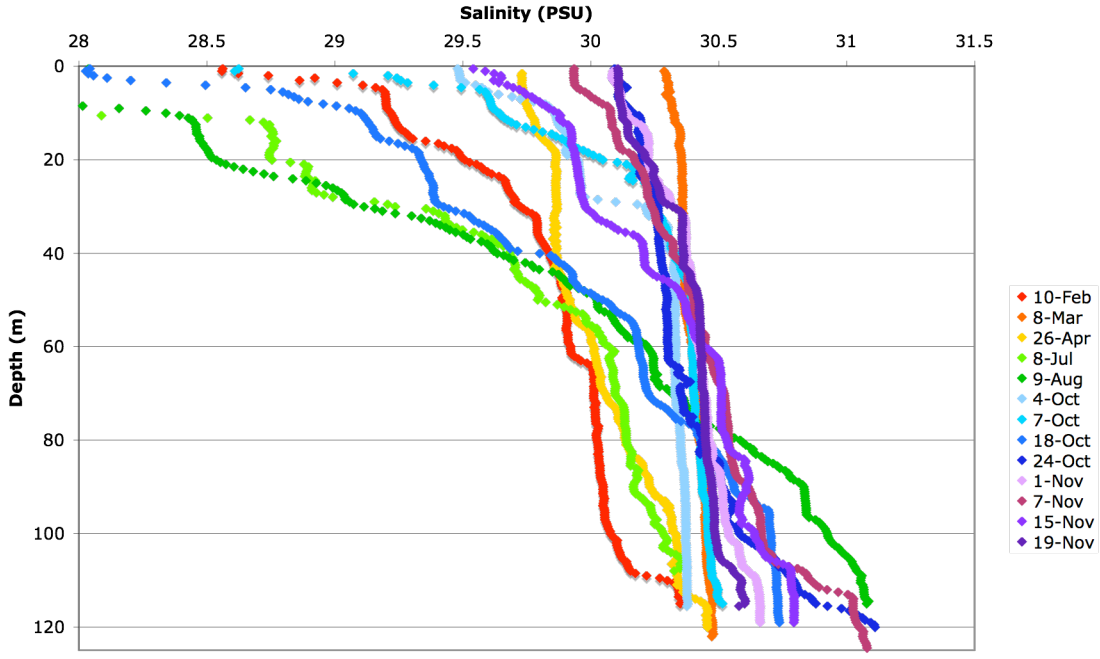

Figure 9: Haloclines at North Station for all of 2011. Salinity axis is truncated to emphasize water column trends deeper than 10m.

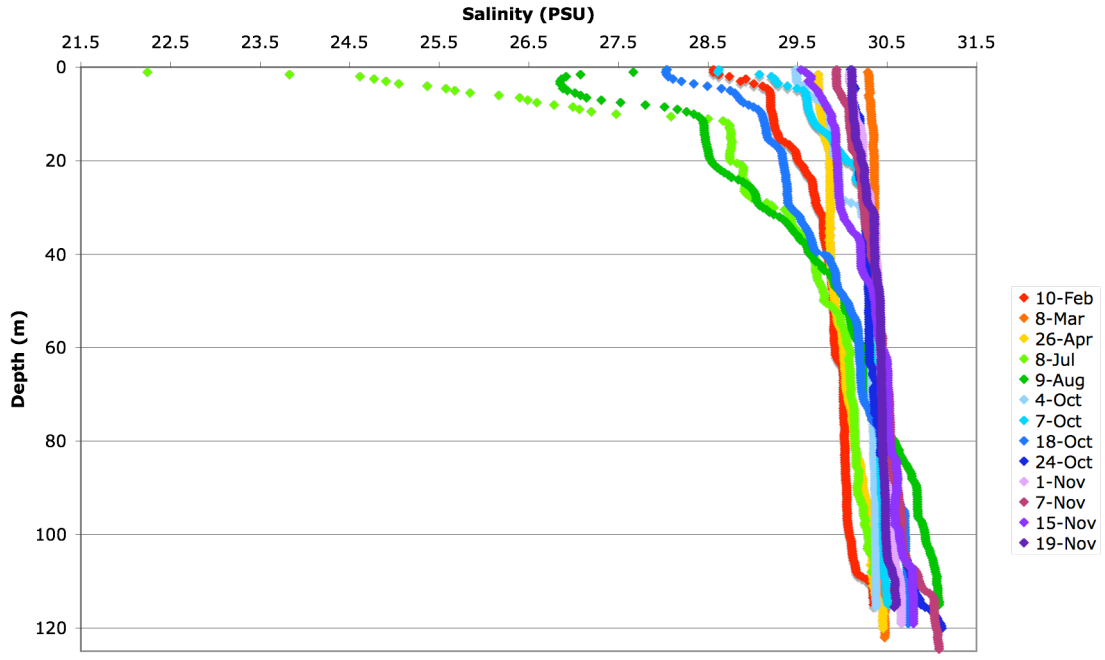

Figure 10: Haloclines at North Station for all of 2011. Salinity axis encompasses the full range of observed values.

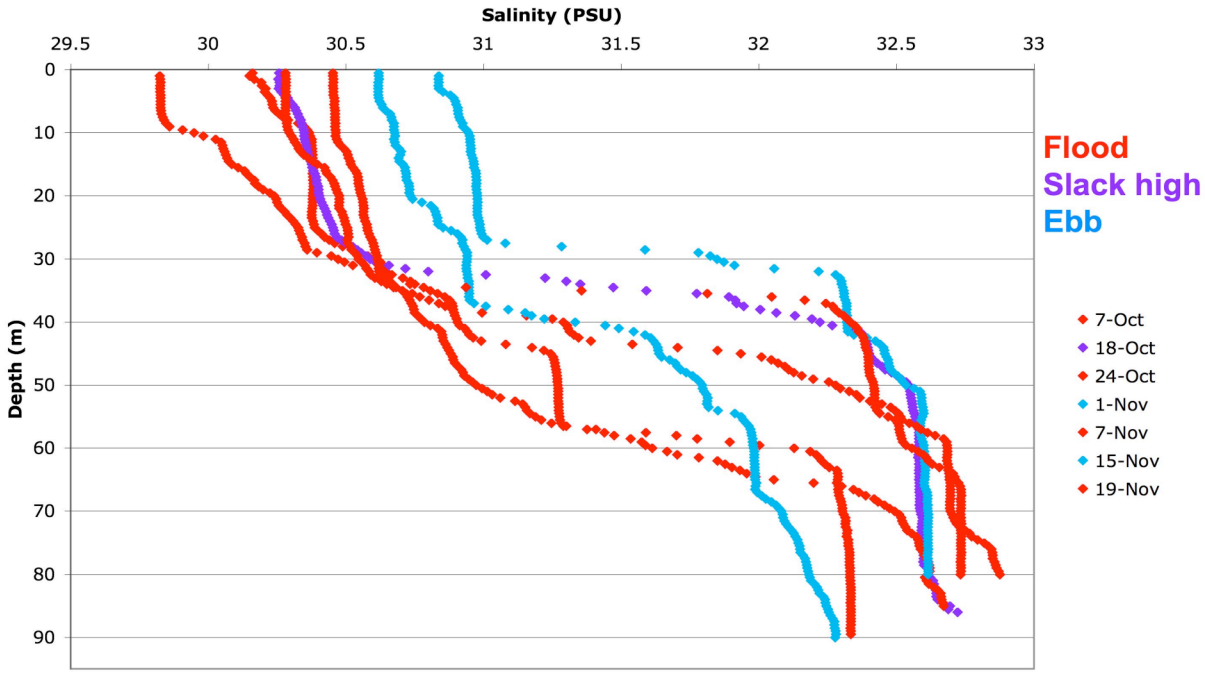

Figure 11: Haloclines at South Station, fall 2011. Flood tides are shown in red, slack high in purple, and ebb tides in blue. The two flood tide haloclines with the saltiest bottom water occurred in November, and the other two occurred in October, all during neap tides.

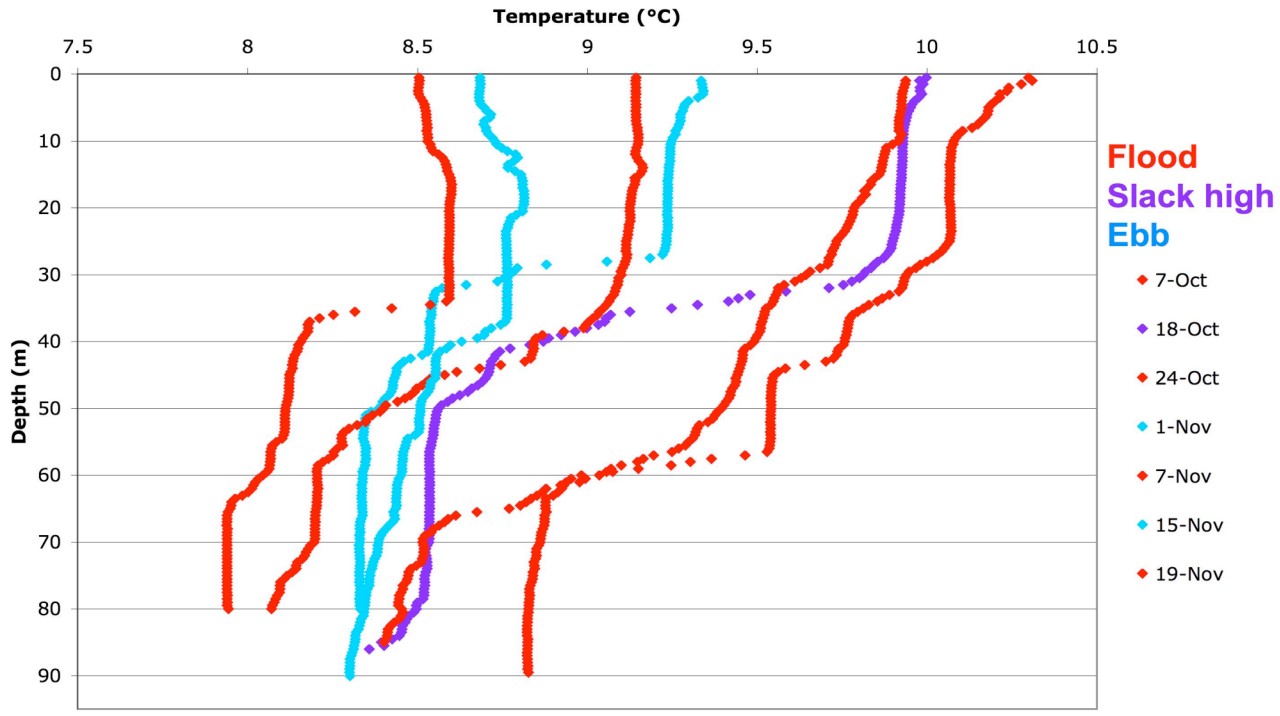

Figure 12: Thermoclines at South Station, fall 2011. Flood tides are shown in red, slack high in purple, and ebb tides in blue. The two flood tide haloclines with the coldest bottom water occurred in November, and the other two occurred in October, all during neap tides.

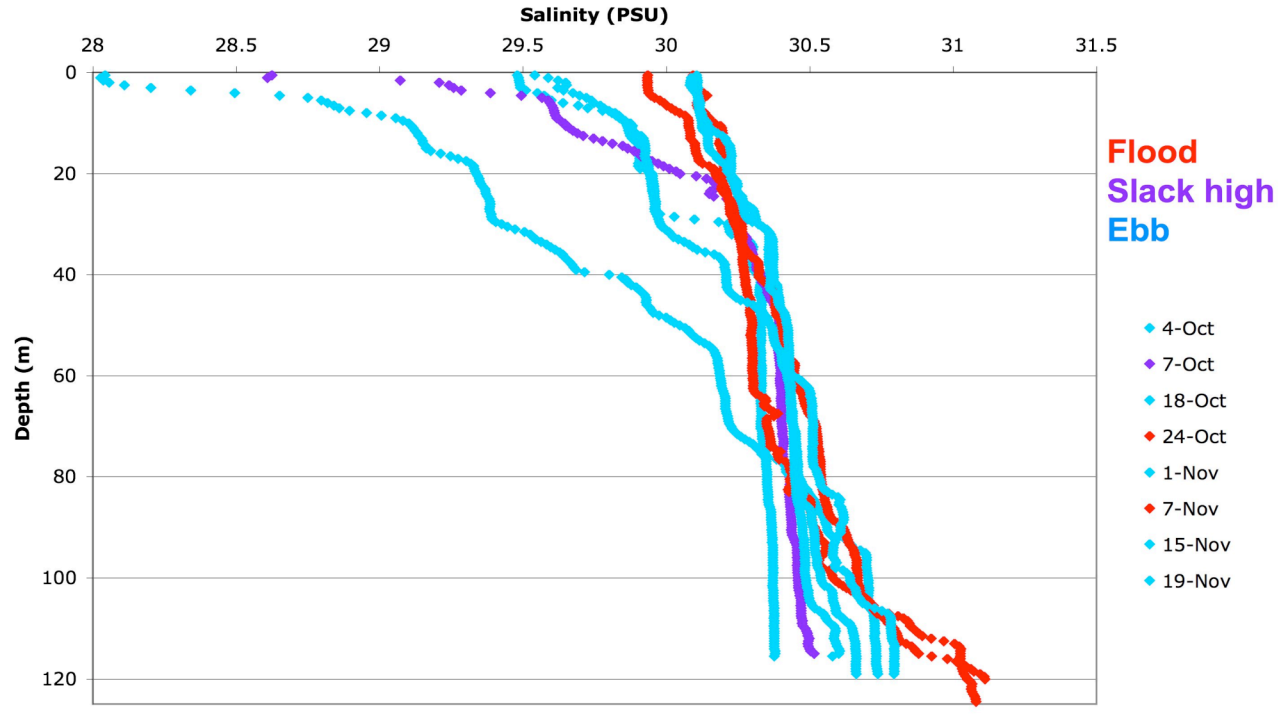

Figure 13: Haloclines at North Station, fall 2011. Flood tides are shown in red, slack high in purple, and ebb tides in blue. Both flood tides were during a neap cycle.

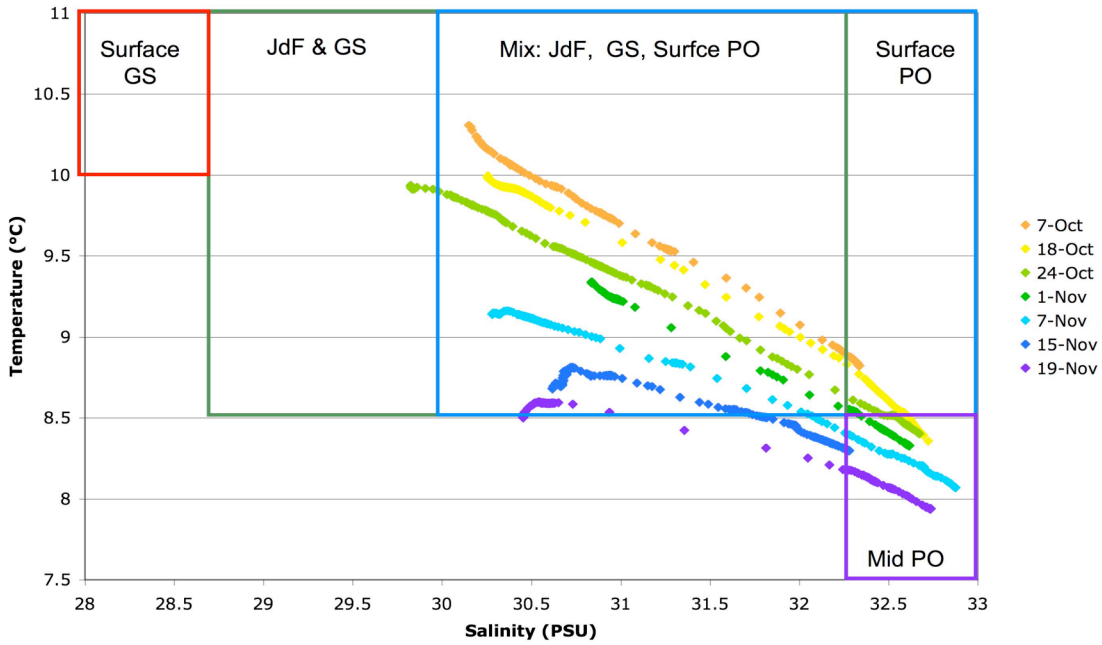

Figure 14: Temperature-salinity plots for South Station, fall 2011. Characteristic temperature-salinity ranges for water origins are shown in boxes. GS=Georgia Strait, JdF=Juan de Fuca Strait, PO=Pacific Ocean.

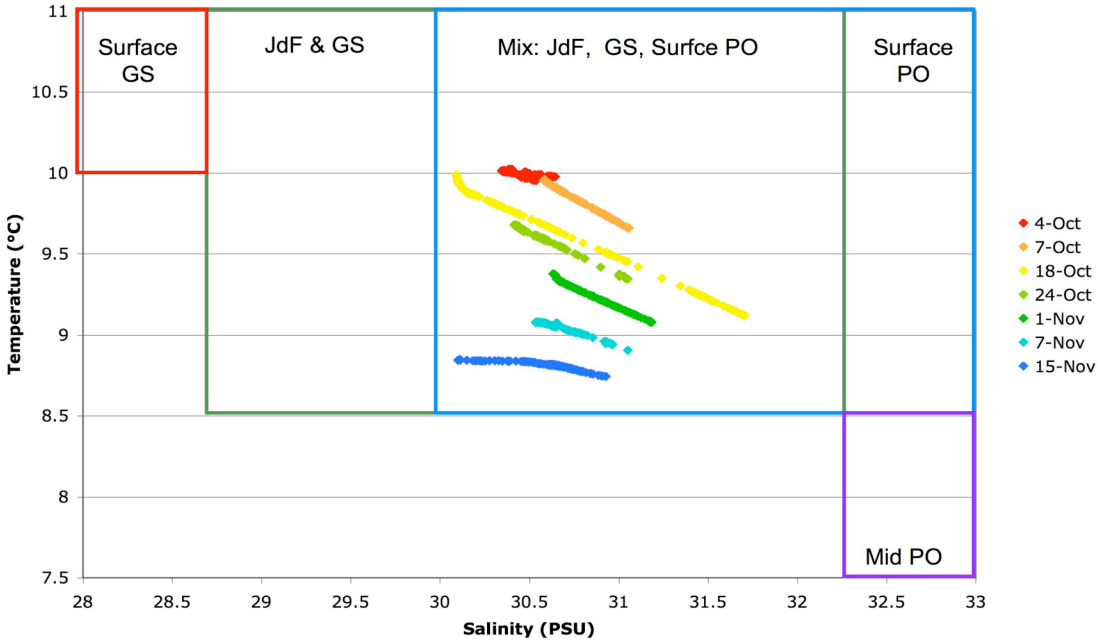

Figure 15: Temperature-salinity plots for Station C, fall 2011. Characteristic temperature-salinity ranges for water origins are shown in boxes. GS=Georgia Strait, JdF=Juan de Fuca Strait, PO=Pacific Ocean.

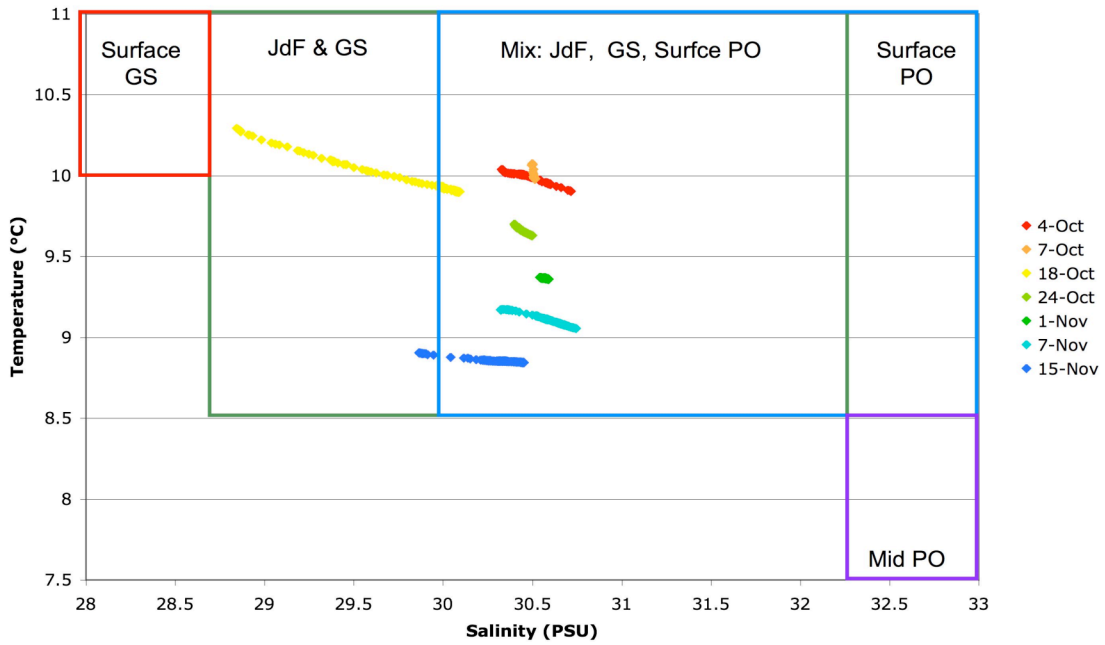

Figure 16: Temperature-salinity plots for Station B, fall 2011. Characteristic temperature-salinity ranges for water origins are shown in boxes. GS=Georgia Strait, JdF=Juan de Fuca Strait, PO=Pacific Ocean.

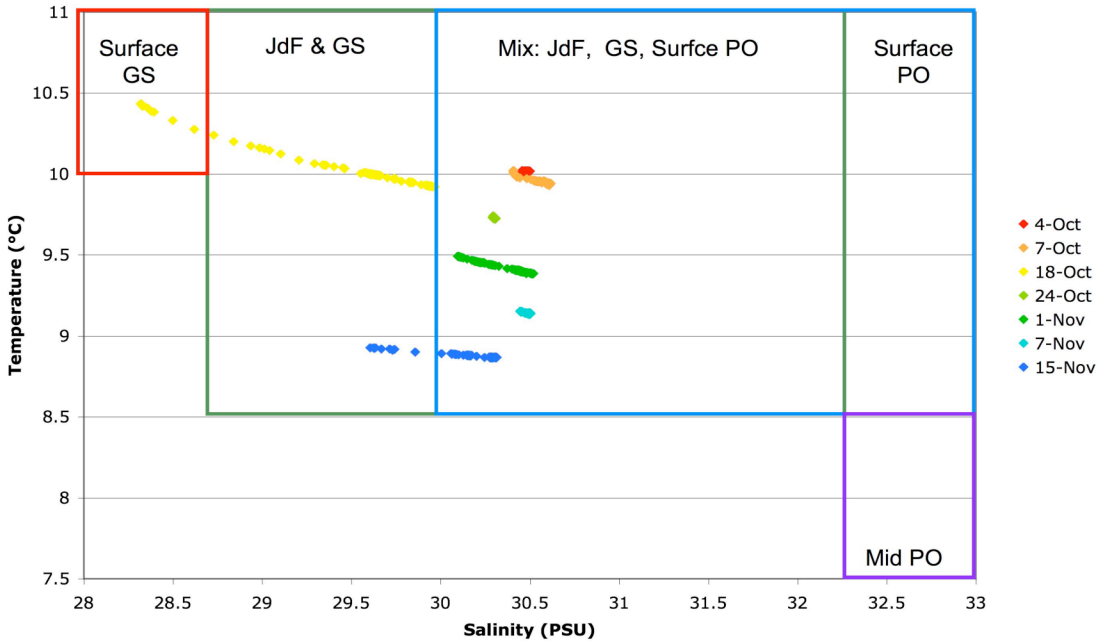

Figure 17: Temperature-salinity plots for Station A, fall 2011. Characteristic temperature-salinity ranges for water origins are shown in boxes. GS=Georgia Strait, JdF=Juan de Fuca Strait, PO=Pacific Ocean.

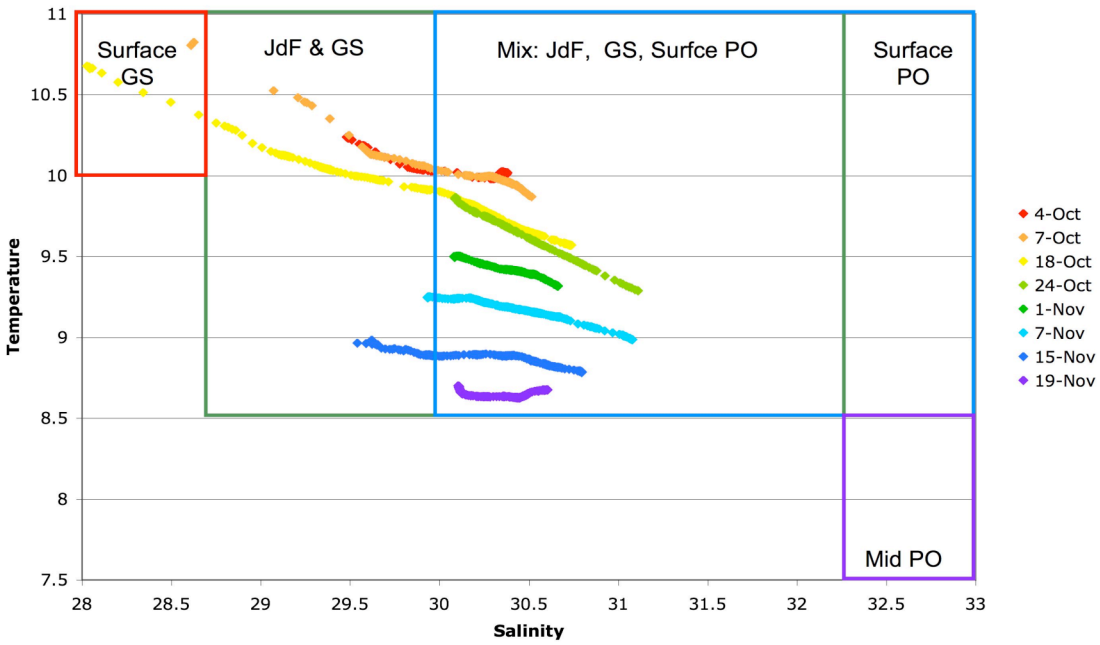

Figure 18: Temperature-salinity plots for North Station, fall 2011. Characteristic temperature-salinity ranges for water origins are shown in boxes. GS=Georgia Strait, JdF=Juan de Fuca Strait, PO=Pacific Ocean.

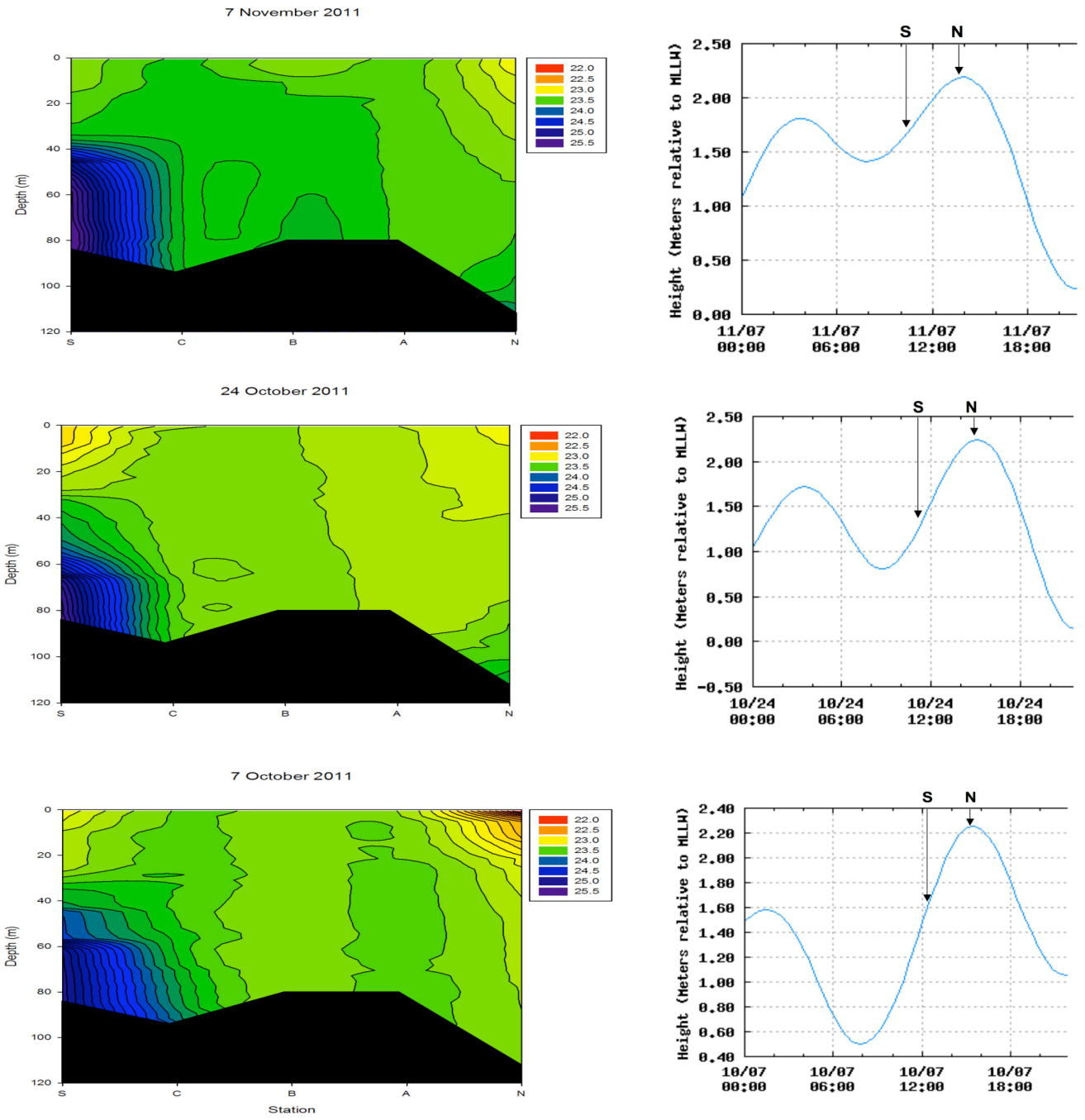

Figure 19: Contour plots of along-channel density (Kg/m^3) during flood tides. Tidal graphs courtesy of the NOAA Friday Harbor station. Sample times of South (S) and North (N) Stations are indicated on tidal graphs with arrows.

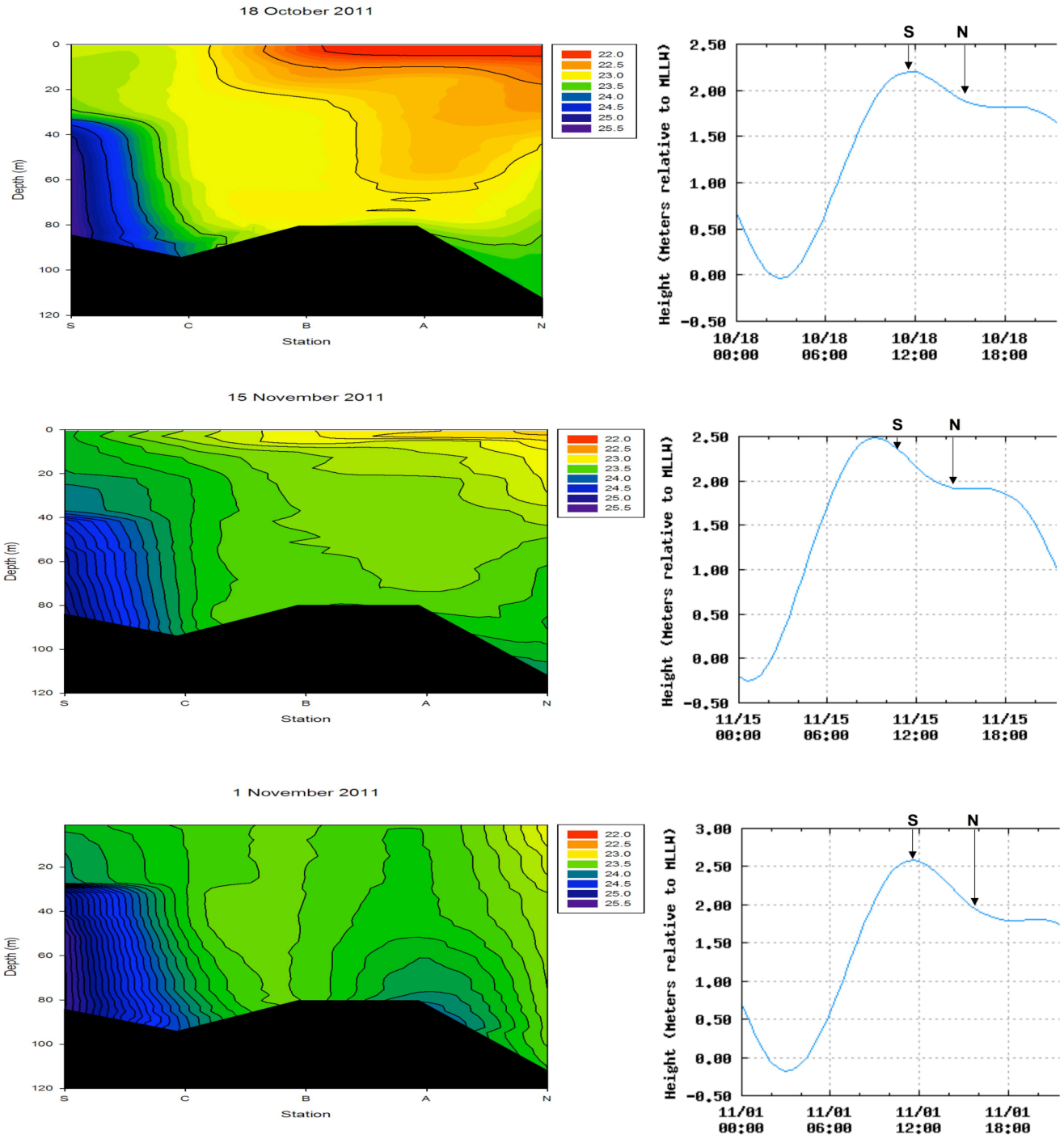

Figure 20: Contour plots of along-channel density (Kg/m^3) during ebb tides. Tidal graphs courtesy of the NOAA Friday Harbor station. Sample times of South (S) and North (N) Stations are indicated on tidal graphs with arrows.

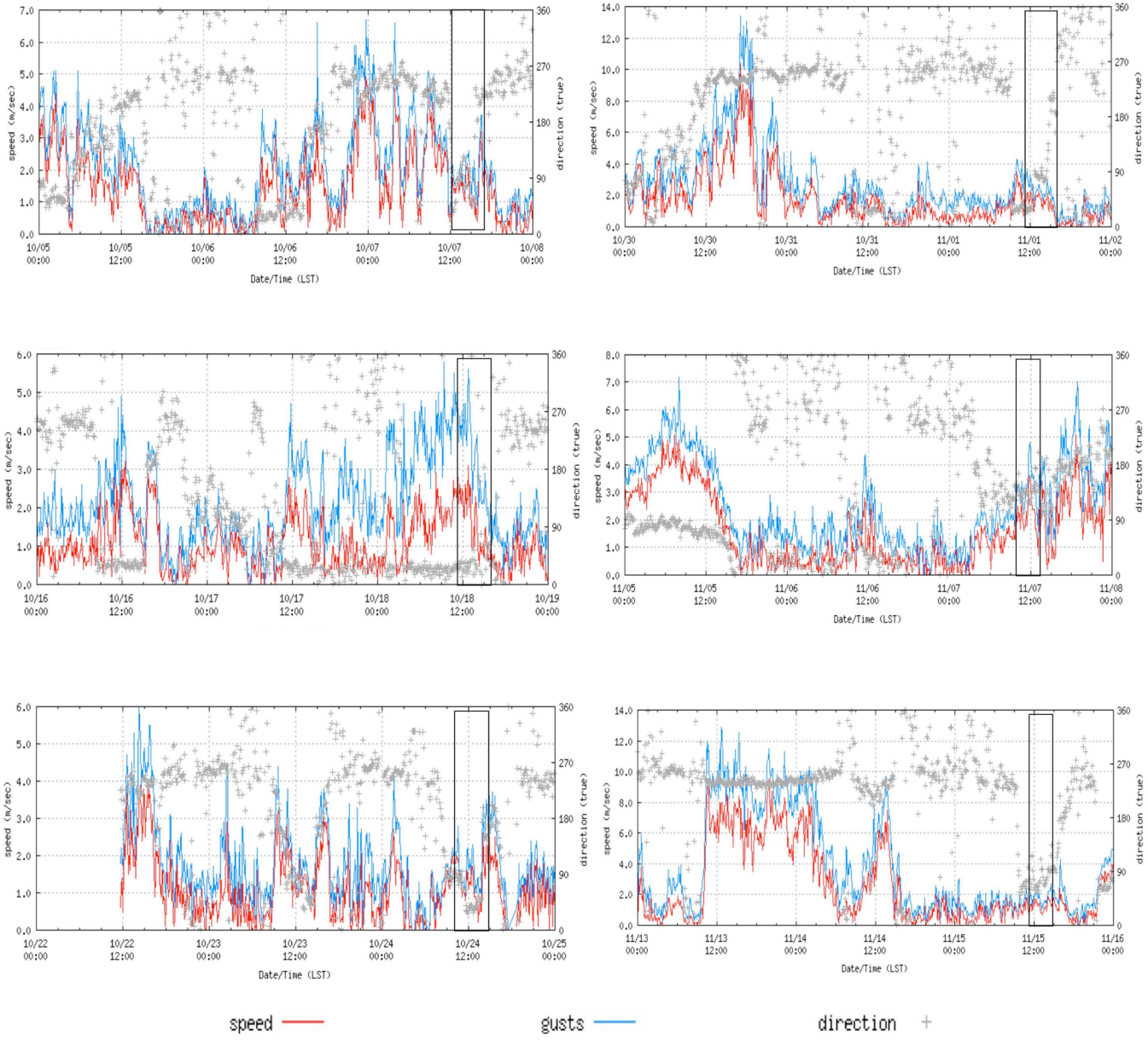

Figure 21: Wind speed and direction preceding and during cruises. Cruise duration indicated by a black rectangle. Wind graphs courtesy of NOAA.

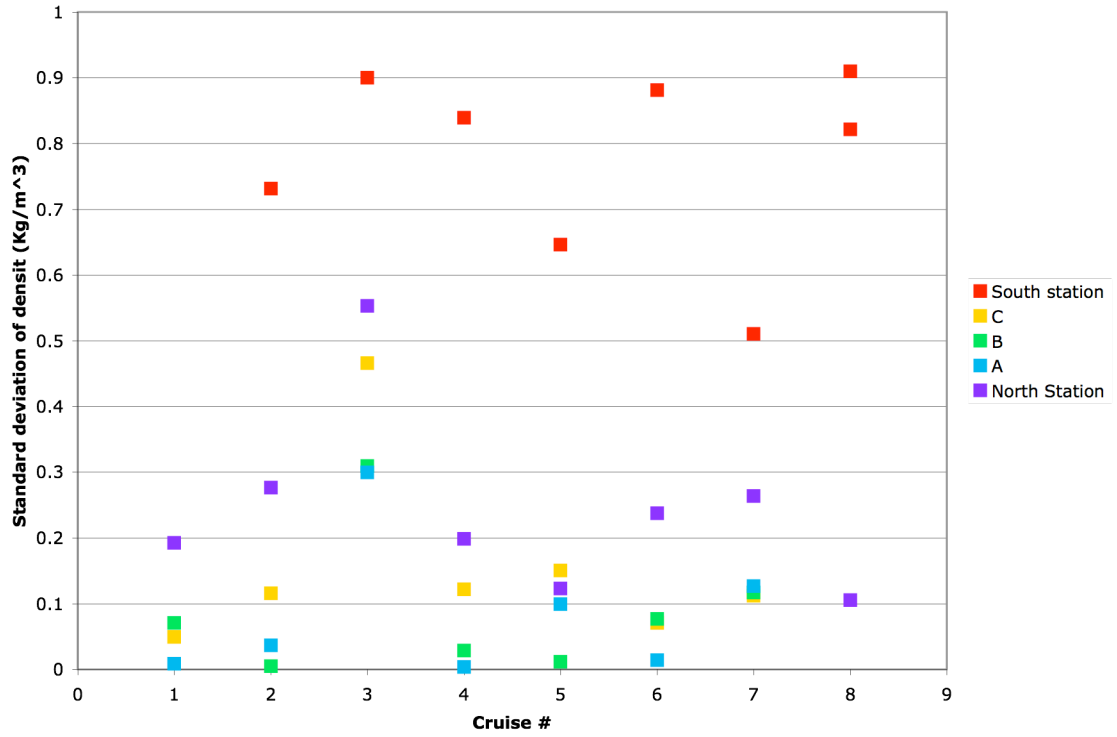

Figure 22: Standard deviation of density at each station for each cruise in fall 2011.

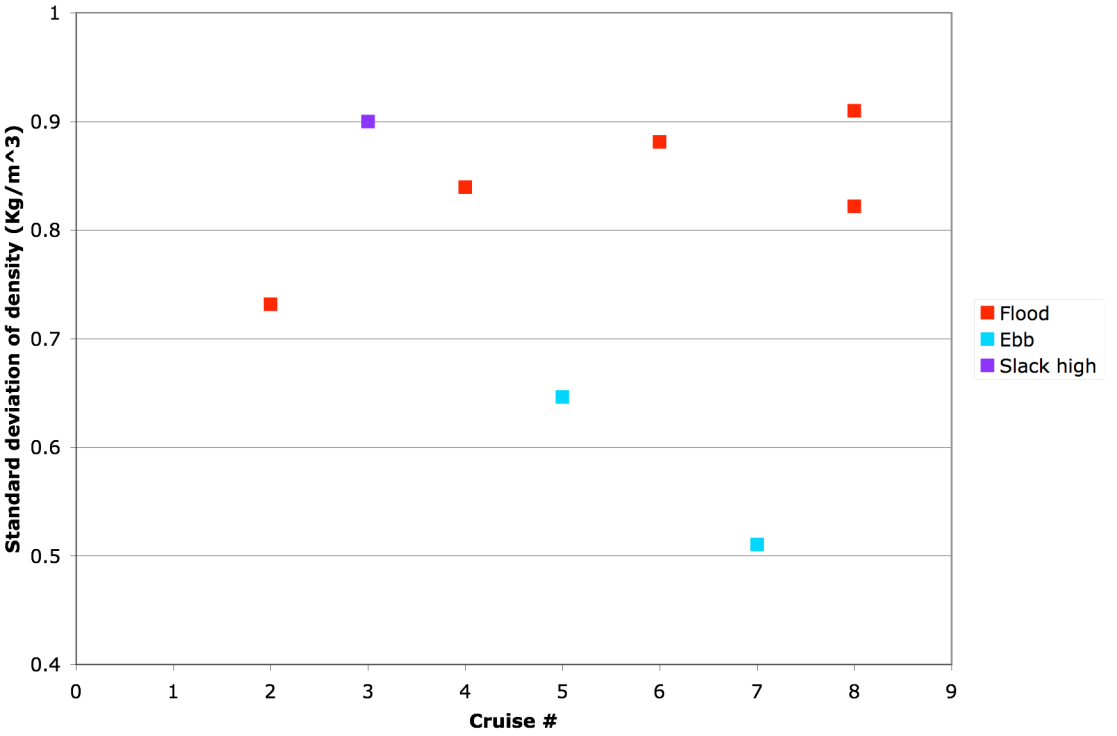

Figure 23: Standard deviation of density during different tidal phases at South Station, fall 2011.

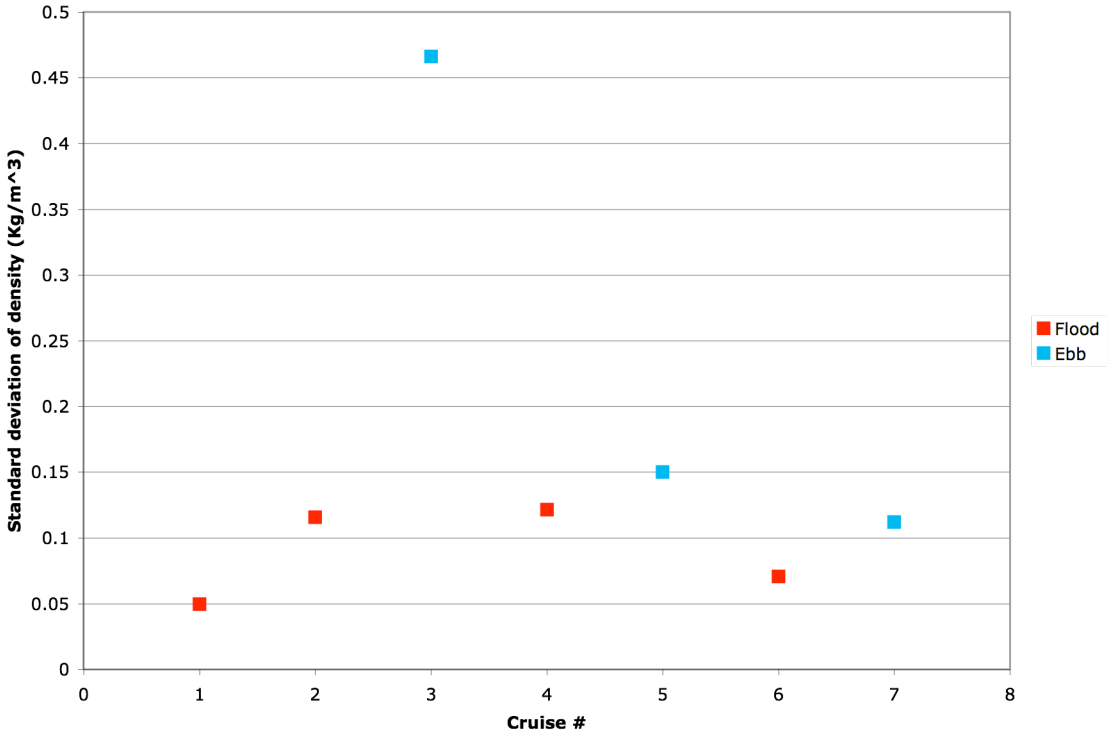

Figure 24: Standard deviation of density during different tidal phases at Station C, fall 2011.

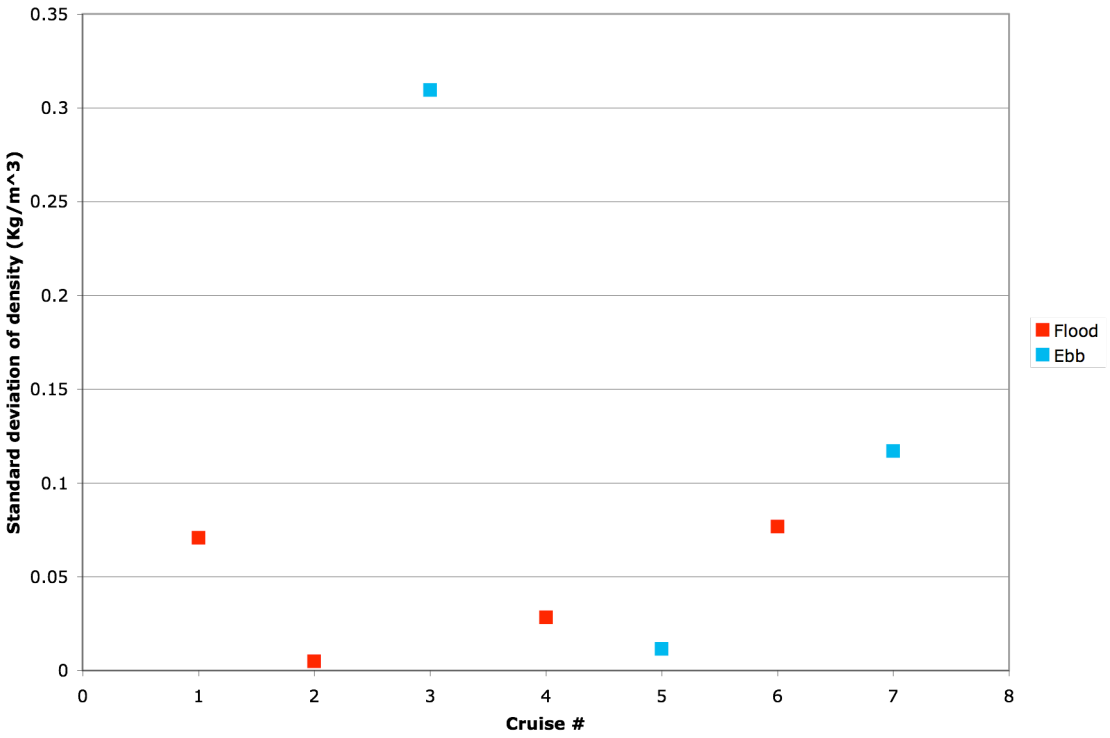

Figure 25: Standard deviation of density during different tidal phases at Station B, fall 2011.

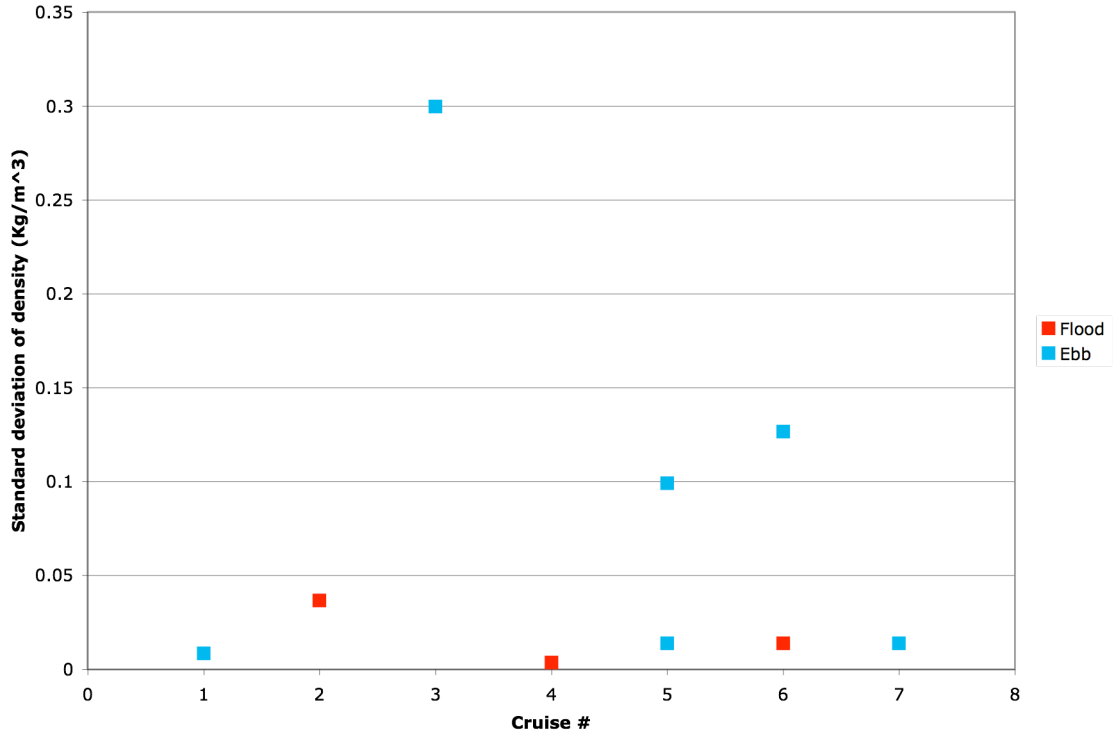

Figure 26: Standard deviation of density during different tidal phases at Station A, fall 2011.

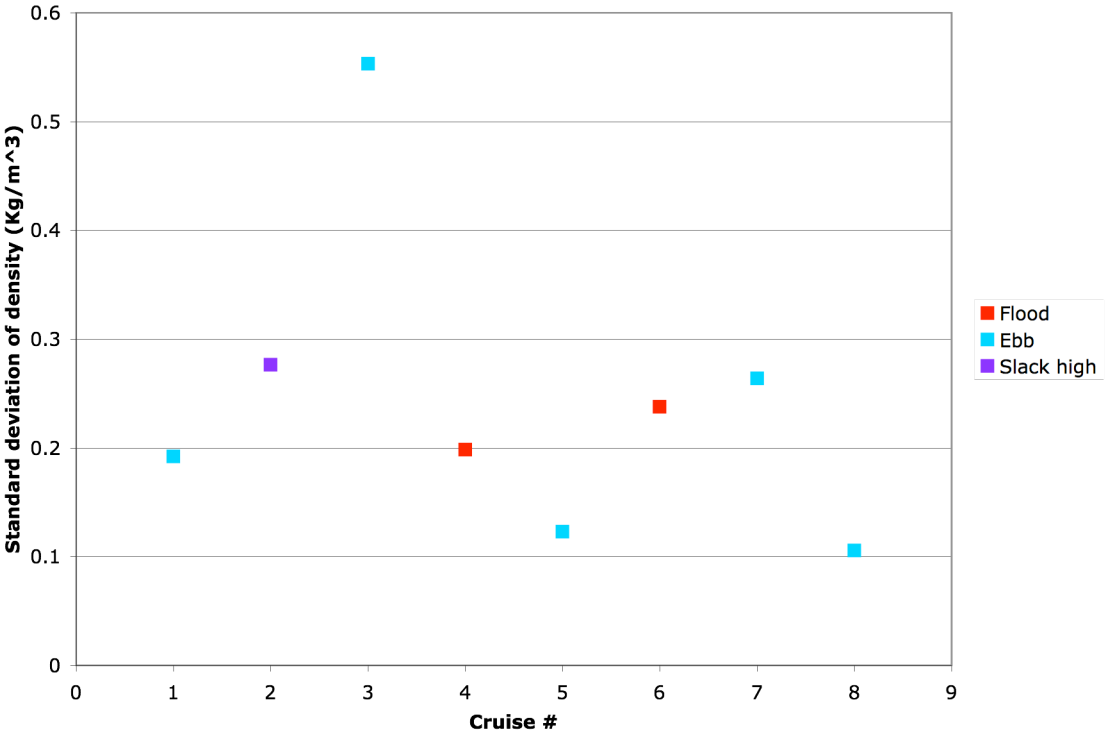

Figure 27: Standard deviation of density during different tidal phases at North Station, fall 2011.

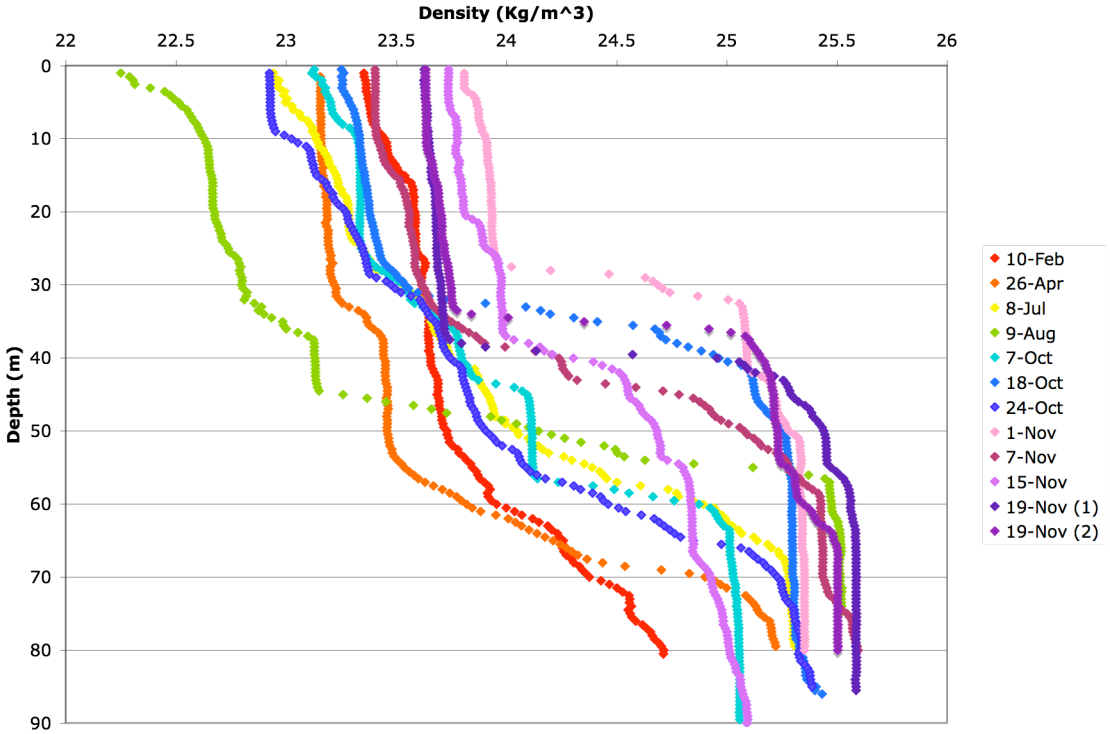

Figure 28: South Station pycnoclines, 2011.

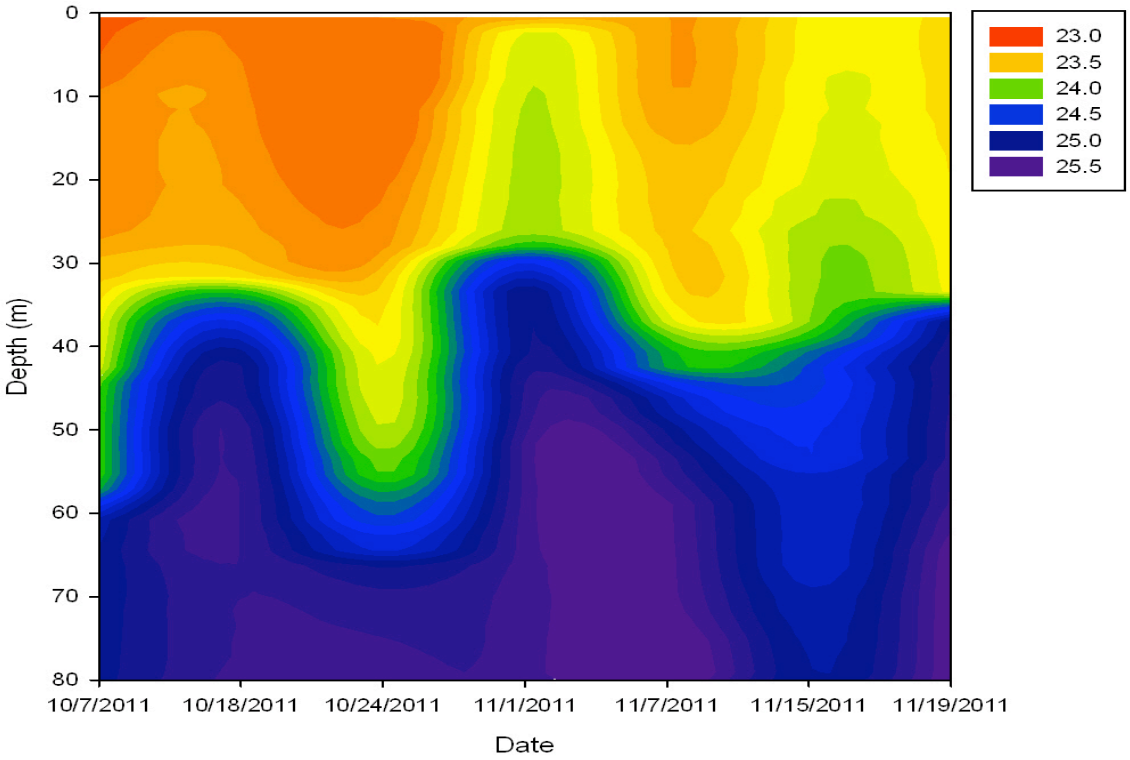

Figure 29: Contour plot of density (Kg/m^3) at South Station by cruise date, fall 2011.

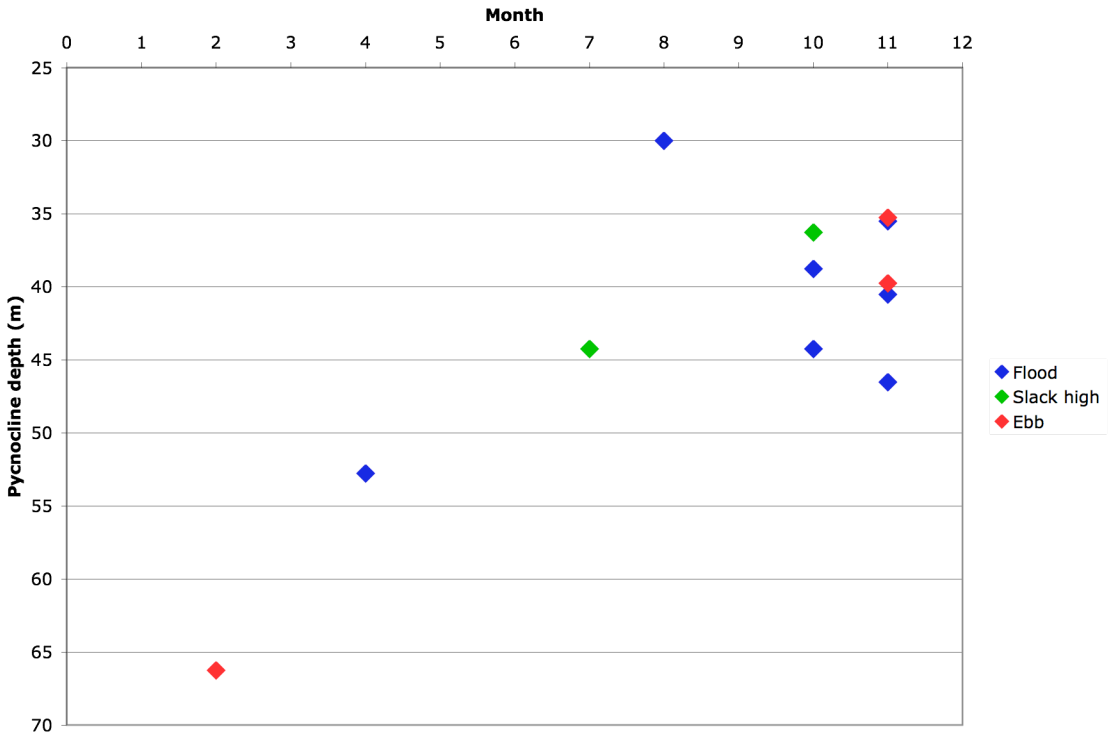

Figure 30: Pycnocline depth vs. month at South Station, 2011.

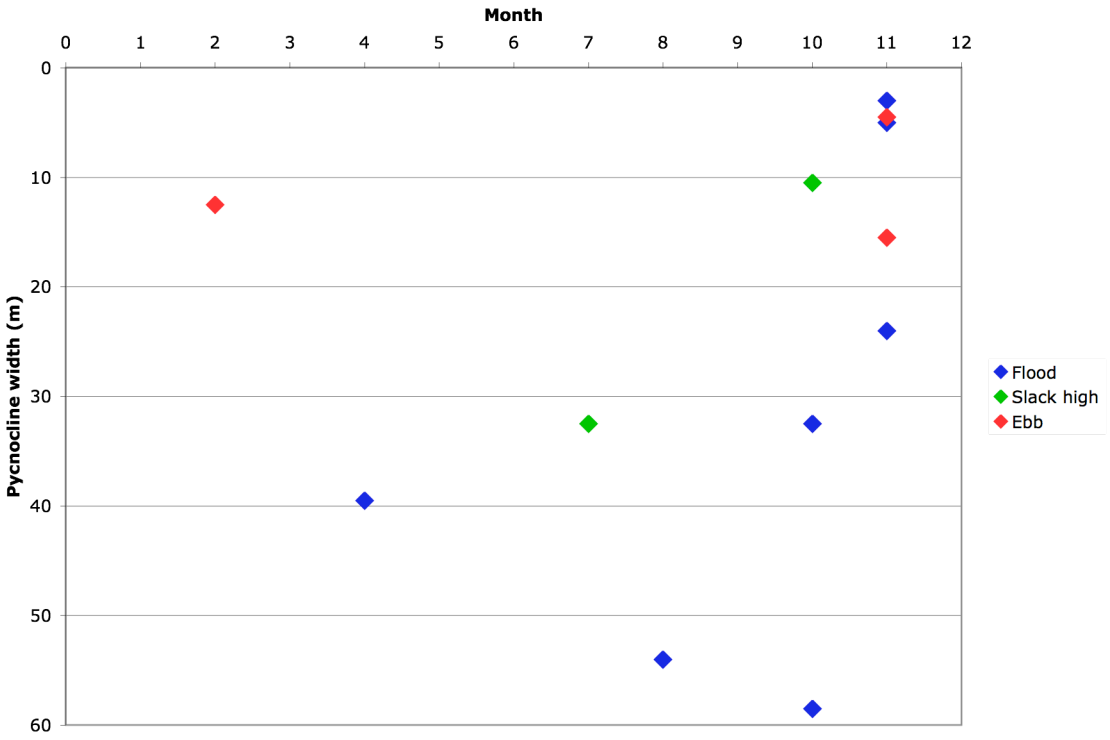

Figure 31: Pycnocline width vs. month at South Station, 2011.

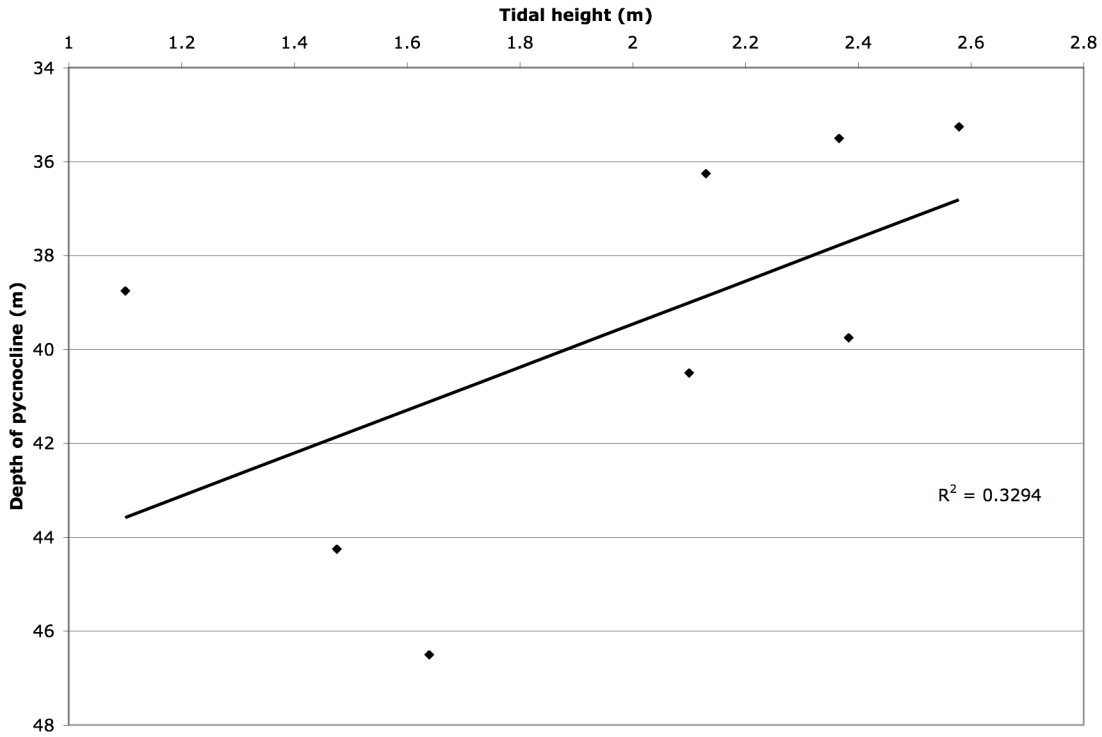

Figure 32: Pycnocline depth vs. tidal height at South Station, fall 2011.

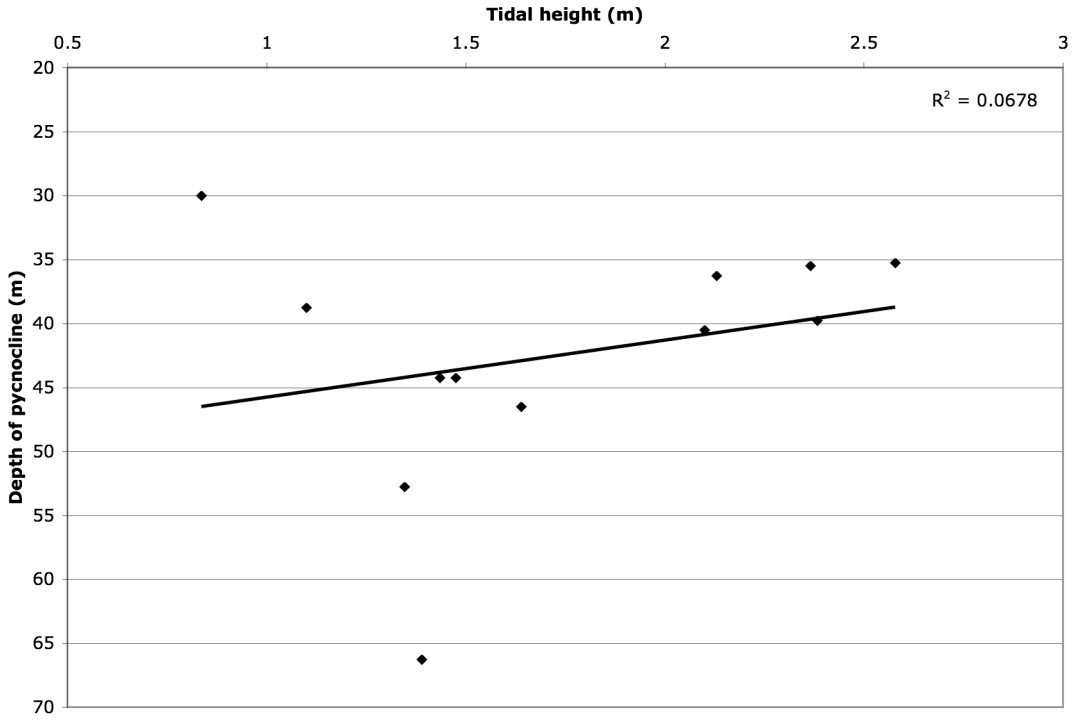

Figure 33: Pycnocline depth vs. tidal height at South Station, all of 2011.

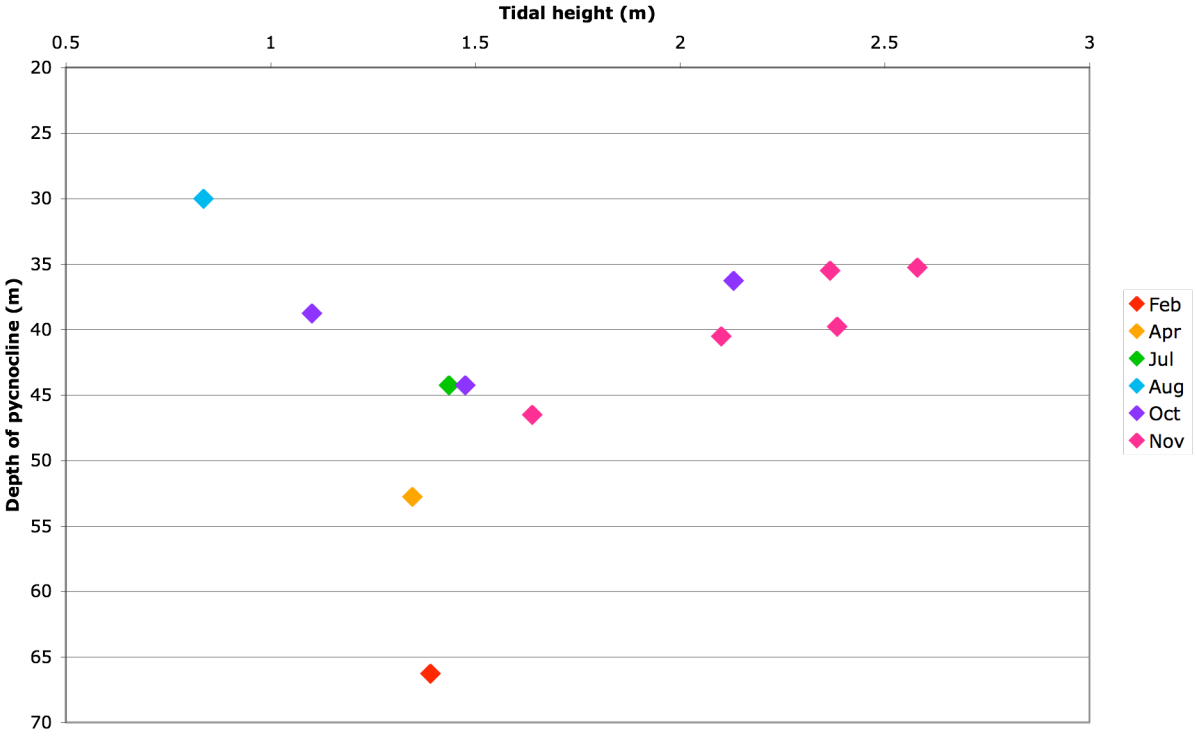

Figure 34: Pycnocline depth vs. tidal height at South Station, all 2011. Data points are color-coded by month.

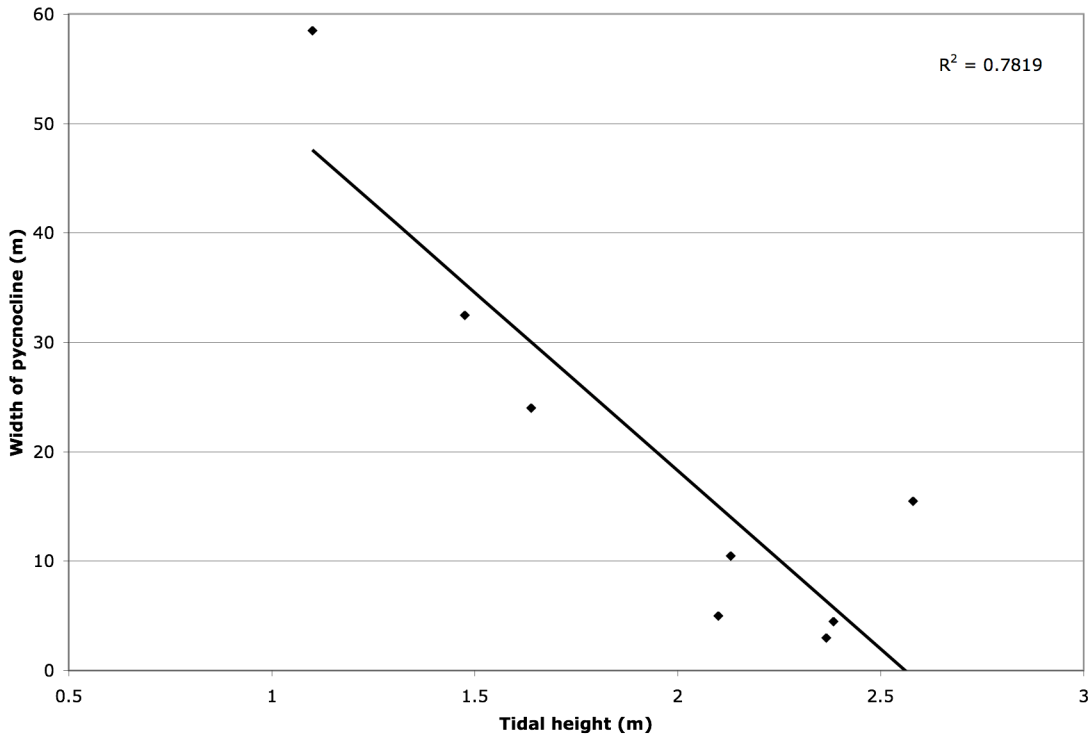

Figure 35: Width of the pycnocline vs. tidal height at South Station, fall 2011.

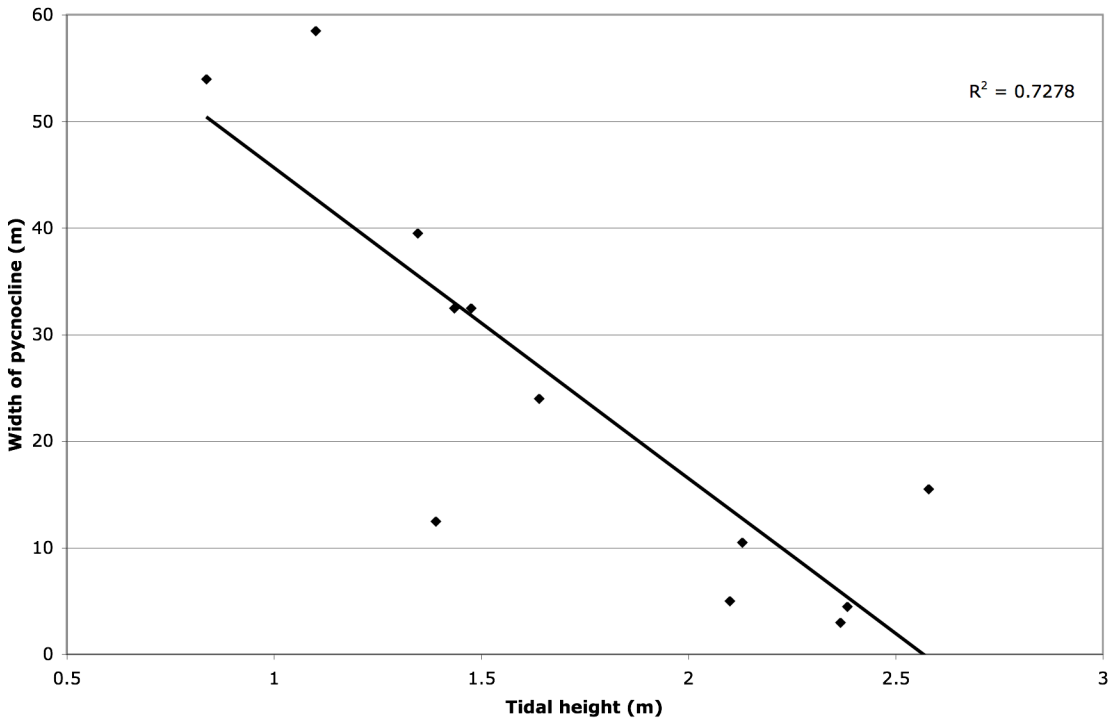

Figure 36: Width of the pycnocline vs. tidal height at South Station, all of 2011.

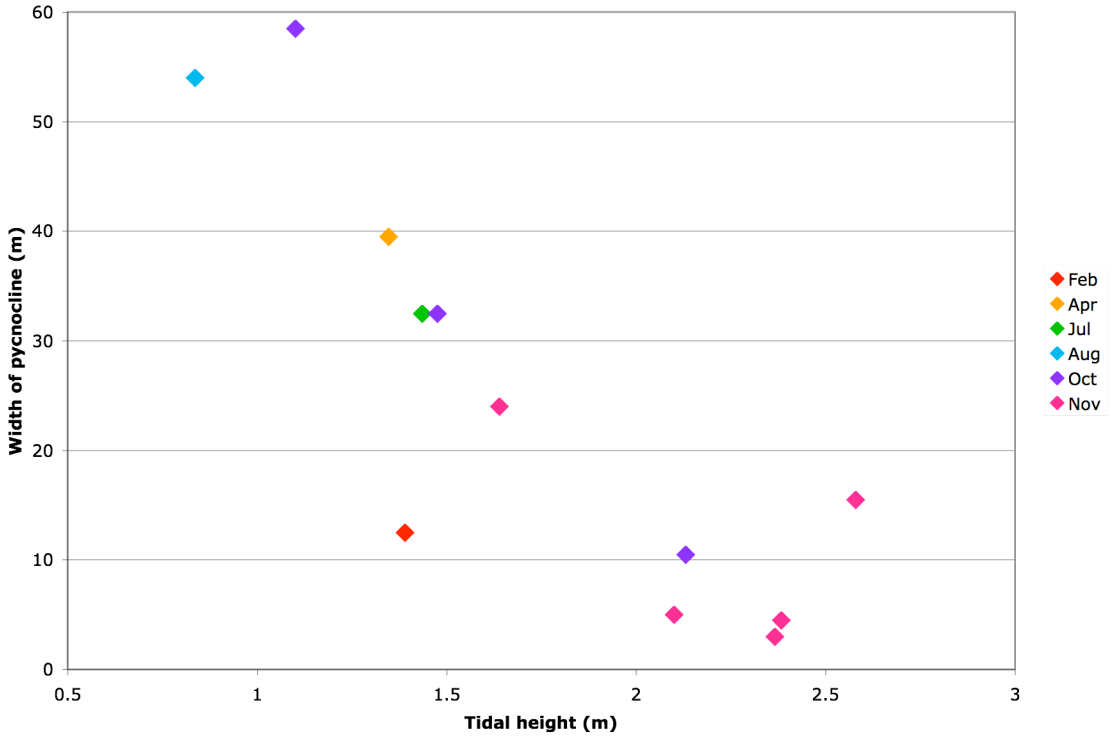

Figure 37: Width of the pycnocline vs. tidal height at South station for all of 2011. Data-points are color-coded by month.